Version of Record: https://www.sciencedirect.com/science/article/pii/S1464343X20300546
Manuscript_1c030a3215a7ab8f0e9b7d275d26ad09

High-resolution sedimentology and sequence stratigraphy of the Oxfordian-Kimmeridgian, Hanifa, Jubaila and Arab outcrops along Jabal Tuwaiq, Central Saudi Arabia

Abdullah Al-Mojel[1, 2], Philippe Razin[2], Guillaume Dera[3]

[1] Saudi Aramco, Dhahran, Saudi Arabia
[2] ENSEGID-Bordeaux INP, EA4592, 33607 Pessac, France
[3] GET, Université Paul Sabatier, CNRS UMR 5563, IRD, OMP, 14 Avenue Edouard Belin, 31400 Toulouse, France

Corresponding author: Email: abdullah.mojel@gmail.com Present address: P.O. Box 5093 Dhahran 31311, Saudi Arabia

Keywords: Sequence Stratigraphy, Late Jurassic, Oxfordian, Mixed carbonate-siliciclastic, Arabian Platform, Inner platform, Epicontinental Sea, Epeiric Sea

Abstract

The sequence stratigraphy of the Late Jurassic (Oxfordian to Kimmeridgian) of the central Arabia is based on outcrop measured sections. The sequence stratigraphic framework is extended eastward across the Arabian Basin through surface-to-subsurface gamma-ray correlations (550 km long to the east). It provides an insight into the development of an intrashelf basin in a large epeiric tropical platform. The outcrop depositional environments range from semi-arid shoreline to carbonate inner-lagoon and back-barrier lagoon. These formed an aggraded flat-topped platform with evident syndepositional differential subsidence. The Upper Jurassic successions are composed of several transgressive third-order sequences interrupted by short emersion sequence boundaries. The Hanifa Platform

© 2020 published by Elsevier. This manuscript is made available under the CC BY NC user license
https://creativecommons.org/licenses/by-nc/4.0/

evolved from proximal argillaceous-limestone with low-faunal diversity to open-marine carbonate platforms with reef bearing and high-faunal diversity adjacent to a deep intrashelf basin in the subsurface. The Hanifa maximum flooding surfaces (MFS's) are placed in terrigenous-free open-marine carbonate sediments. The Jubaila-Arab-D is a conformable succession marked at the base by storm-influenced inner-platform grainstones with quartz sandstone, and proximal barren lime-mudstone. The Jubaila-Arab-D MFS is placed higher in the Arab-D reservoir in a backstepping of back-barrier high-energy reef facies. During sea-level highstand, the reef facies are gently prograding toward the Rimthan Arch leaving behind a restricted lagoon deposits consists of sabkhah/salina anhydrite. These composite sequences are probably controlled by climatic driven eustasy, coupled with local tectonic disruption, as they have some similarity with other Tethyan sequence stratigraphy. For the first time, this outcrop study reveals a detailed and complete stratigraphic framework that subdivided the Upper Jurassic prolific petroleum systems into genetically related sequences that are not always obvious from subsurface data. The study allows the assessment of the Upper Jurassic tectono-stratigraphic events of the central Arabian Platform.

1 Introduction

The Upper Jurassic outcrops are very well exposed in central Arabia along the Tuwaiq Escarpment (Fig. 1). In the subsurface, the studied interval hosts the world's most prolific hydrocarbon reservoirs, Hanifa and Arab-D, and a significant source rock interval in the Hanifa Formation (Powers, 1962; Powers et al., 1966; Powers, 1968; Murris, 1980; Droste, 1990; McGuire et al., 1993; Al-Naji, 2002).

Prior to this study, the outcrops of the Hanifa Formation, Jubaila Limestone and Arab-D Member were subdivided into several large mapping units based on lithostratigraphic and biostratigraphic correlations (Powers et al., 1966; Powers, 1986; Manivit et al., 1990). Genetically related depositional sequences were not documented in detail. The depositional environments of the most productive reservoirs in Saudi Arabia, Arab-D, are the subjects of long-standing debate, which has been proposed as either a deep basinal or shallow lagoonal depositional setting (Powers, 1962; Mitchell et al, 1988; Meyer and Price 1993; Handford et al., 2002; Lindsay et al., 2006; Al-Awwad and Collins, 2013b). The progradational direction of the Arab-D reservoir is a controversial topic as it has never been demonstrated convincingly (Mitchell et al., 1988; Meyer and Price, 1993; Handford et al., 2002; Lindsay et al., 2006; Al-Awwad and Collins, 2013b). Additionally, previous lithofacies and biofacies of the Hanifa outcrop were interpreted to be depth-dependent and, accordingly, they were distributed on a ramp platform (e.g., poor-fauna argillaceous lime-mudstone is deep and distal, grainstone is shallow and proximal); and so their vertical facies changes were attributed solely to relative sea-level variation (Hughes et al., 2008; Al-Mojel and Kerans, 2014; Fallatah and Kerans, 2018). This practice could mislead the sequence stratigraphic interpretations, especially where system tracts and facies migration are concerned. This study focuses on a new depositional model with emphasis on the influence of tectonics, eustasy and platform physiography on depositional conditions. These issues need to be addressed and brought out clearly in a new and complete sequence stratigraphic study. Our approach is to integrate, for the first time, the previous biostratigraphic data with detailed sedimentological measured sections and subsurface gamma-ray logs. This allows assessment of the unique physiography of the Arabian Platform and the controlling factors, which promoted the development of carbonate platform and facies distribution and its stratal architecture.

2 Geological Setting

2.1 Tectonic and paleogeographic setting

The study area was located on the eastern side of the Gondwana (Fig. 2). The Arabian Plate during the Late Jurassic faced the Neo-Tethys Ocean with a slowly subsiding intracratonic passive margin with tropical epeiric shallow-marine deposits (Murris, 1980). The study area was at this time in the proximal part of the Arabian Platform, close to marginal marine siliciclastic facies belt and more than 1000 km landward from the Neo-Tethys continental margin (Ziegler, 2001).

The Middle-Late Jurassic transition was probably a time of tectonic instability and tilting. Incipient breaking of the Arabian-Indian plate boundary is marked by a volcanic interruption in eastern Oman (Ziegler, 2001; Al-Mojel, 2017). The tectonic instability probably extended to the Late Oxfordian-Early Kimmeridgian time. Evidence of post-deposition broad erosion and exposure south of Iraq (southern Gotnia Basin) was attributed to basement faulting and uplift (Sadooni, 1997, in Ziegler, 2001). In Yemen, active rifting commenced in the Early Kimmeridgian and lasted up to the Tithonian; marked here by a thick succession of open-marine deposits (Brannan et al., 1999; Ahlbrandt, 2002).

2.2 Stratigraphic setting

2.2.1 Hanifa Formation

The basal boundary of the Hanifa Formation corresponds to a stratigraphic hiatus over the Tuwaiq Mountain Limestone and covering the lower part of the Oxfordian (*mariae* Zone) (Le Nindre in Kadar et al., 2015). The top boundary of the Hanifa Formation is considered as a conformable surface (Powers, 1968; Manivit et al., 1990). The Hanifa Formation is subdivided into two formal members; the Hawtah (H1) and the overlying Ulayyah (H2) members (Vaslet et al., 1983; Fig. 3). The lower part of the member is attributed to the Early Oxfordian (*cordatum* Zone?) based on brachiopod fauna (*Ornithella* gr. *hudlestoni* DAV.) and on nautiloids (*Paracenoceras* sp. aff. *arduennense*; Ar Rawdah section in Manivit et al., 1990). The only confirmed ammonite zone in the Hanifa Formation is Middle Oxfordian (*plicatilis* Zone) based on ammonite fauna (*Euaspidoceras catenaperarmatum* and *Perisphinctidae*?), nautiloids (*Paracenoceras* aff. *hexagonum*) and nannoflora (*Vekshinella stradneri*) present in the upper part of the Hawtah Member (Manivit et al., 1990).

The Ulayyah Member shows generally the first appearance of the foraminifer *Alveosepta jaccardi* Schrodt. No ammonites have been found in the Ulayyah Member. The lower half of the member is dated Late Oxfordian based on foraminifera (*Alveosepta Jaccardi*) and on brachiopods (*Terebratula bisuffarcinata*; Manivit et al., 1990). The upper half is dated Early Kimmeridgian based on echinoids (*Monodiadema kselensis* and *Pseudocidaris thurmanni*) and *Alveosepta Jaccardi* (Manivit et al., 1990).

2.2.2 Jubaila Limestone

The Jubaila Limestone conformably overlies the Hanifa Formation (Manivit et al., 1990; Powers, 1968). This formation is subdivided into two informal units – the J1 and the overlying J2 (Manivit et al., 1985b; Fig. 3). This lower unit is dated Early Kimmeridgian based on nautiloids (*Paracenoceras* gr. *hexagonum, Paracenoceras* aff. *wepferi*) and endemic ammonites (*Perisphinctes* aff. *Jubailensis*) (Manivit et al., 1990). The Jubaila Formation is conformably overlain by the Arab Formation (Arab-D Member; Manivit et al., 1990).

2.2.3 Arab Formation, Arab-D Member

The Arab Formation is subdivided into four members A-D, in descending order (Steineke et al., 1958). The base contact of the Arab Formation definitions is picked differently at outcrop and in the subsurface (Appendix 1). The Arab-D Member ends with collapse breccia interval below the Arab-C Member. The breccia is due to the dissolution of anhydrite between the Arab-D and Arab-C Member, which have been lately defined as Arab-D Anhydrite (*sensu* Mitchell et al., 1988; Appendix 1). The Arab Formation lacks ammonites and is dated as Kimmeridgian to Tithonian based on microfaunal association including benthic foraminifera (Manivit et al., 1990; Hughes, 2009) and by lateral equivalence (Thierry et al., 2000).

3 Methods

This sequence stratigraphic study is based on 14 sedimentological sections (Fig. 1), with a total thickness of 1500 m, and 120 stained thin section samples. The sedimentological data include: mineralogy, color, sedimentary structures, extended Dunham texture (Dunham, 1962; Embry and Klovan 1971), grain types, grain size, and fossil types and bioturbation.

High-resolution stratigraphic correlations have been defined using field physical correlation and sequence stratigraphic concepts. The sedimentological-based sequences are defined in outcrop and have been extended to the main hydrocarbon fields in the subsurface in a cross-section using gamma-ray logs.

The sequence stratigraphic cross-sections are complemented with biostratigraphic data of Manivit et al. (1990). The cross-section of the Jubaila and Arab-D Member is supplemented with an additional measured section (Wadi Al Majami, 21° 04’ N) from Vaslet et al. (1985).

4 Facies and depositional environment

The regional facies distribution is shown in figures (4 and 5). The spatial distribution of the facies are shown in sequential depositional models (Fig. 11 and 12) that illustrate the evolution of the depositional systems in response to a third-order relative sea-level changes. Eleven facies or facies associations have been recognized within the Hanifa Formation, Jubaila Limestone and Arab-D Member. The descriptions of the sedimentary facies are summarized in Table 1 and the interpretation of their depositional environments are discussed below. The facies are grouped in four depositional environments, which comprise from proximal to distal: arid shoreline, mixed carbonate-siliciclastic inner-lagoon, carbonate inner-lagoon and back-barrier lagoon.

The facies analyses give important indications for interpreting the mechanism of sedimentation and depositional environments. The interpretation of depositional environments are not always unequivocal, particularly with regard to the water depth and lagoonal versus offshore setting of some facies. This is because the depositional system is complex as it evolves through time within a depositional sequence and during the whole Late Jurassic period. Therefore, the interpretation of the depositional environments went through an iterative process between facies description, vertical and lateral facies distribution and relationships by using Walther's Law, stratigraphical geometry (clinoform versus tabular or parallel) and paleogeographical location of the facies.

4.1 Arid evaporitic shoreline and lagoon

F1: Anhydrite solution collapse breccia: subaqueous salina

This facies occur only at the top of the Arab-D Member (Fig. 6A and B) and is equivalent to the Arab-D Anhydrite in the subsurface (Sharief et al., 1991). These units exhibit karstic collapse features and highly deformed rotated units, and are interpreted to be formed mainly in a subaqueous salina (McGuire et al., 1993; Handford et al., 2002; Lindsay et al., 2006), and to a lesser extent, in a sabkha depositional environment (Al-Awwad and Collins, 2013a) prior to dissolution and collapse.

F2: Red dolomite: tidal-flat to restricted lagoon

These dolomitic beds are interpreted to form in response to highly evaporitic conditions in restricted tidal-flat and lagoons, associated with periods of non-deposition (Swart et al., 2005). The increase in occurrence of dolomite facies around the sequence boundaries suggests a control of low accommodation rates on the formation of the dolomites.

4.2 Mixed carbonate-siliciclastic inner-lagoon

F3: Cross-bedded quartz sandstone: shallow-marine sand-flat

They are interpreted as shallow-marine sand-flat deposits. The plane and wave-ripple laminations attest to wave generated currents in an upper shoreface setting (cf. Reynolds, 1995). The intimate occurrence above the depositional-related red dolomite beds (F2) suggest that the laminated sandstones were deposited in a proximal setting, beach or shoreline environment. The interfingering of low-energy lime-mudstone facies (F6) indicates that a time of storm-generated currents are frequent and wave-base is probably relatively shallow.

F4: Calcareous shale and argillaceous lime-mudstone to packstone: shale-dominated inner-lagoon

This low-energy facies is interpreted to be deposited in shale dominated shallow-marine inner-platform setting. The terrigenous content is related to both the reworking of shale deposits during early-transgressive process and to a paleogeographical location close to the terrigenous influx. The associated storm-generated grainstone beds suggest that the inner platform was occasionally influenced by storm events. The predominance of *Chondrites* burrows and the associated low-faunal diversity (Appendix 2 and 3) imply an overall restricted low-oxygenated bottom waters (Bromley and Ekdale, 1984; Goldring et al., 2005), which could be attributed to the proximality to hinterland freshwater runoff and high-nutrient supply with resultant oxygen stratification (Bottjer et al., 1986 in Read, 1989; Rabalais et al., 1991; Lukasik et al., 2000).

F5: Nodular bioturbated peloidal wackestone/mudstone: inner lagoon

The fine-grained deposits indicate low energy background condition, while the heterolithic stratification and the alternation of lime mudstone and grainstone suggest intermittent storm and current influence. As the bioturbation has largely destroyed the physical sedimentary structure, it is difficult to identify the type of current controlling the deposition. Intercalations of storm beds are probably present suggesting a low energy wave dominated environment with record of some higher amplitude storm events. Unfortunately, there are no direct sedimentological or biofacies evidence to discriminate between deep-water upper-offshore environment or shallow-marine protected inner-platform setting.

4.3 Carbonate inner-platform

F6: Thinly laminated barren lime-mudstone: restricted inner-lagoon

These barren and non-bioturbated lime-mudstones are interpreted to be deposited in a restricted poorly oxygenated inner-lagoon occasionally subjected to high-energy storm pulses. The low-angle laminations suggest episodic wave and current action at speed reaching 50 cm/sec (Schieber et al, 2007; Schieber et al., 2013; Al-Awwad and Pomar, 2015; Frébourg et al., 2016). The deposition of such barren thick shallow-water lime-mudstone is probably influenced by cyanobacterial photosynthesis process as part of the Jurassic neritic lime-mud factory (Pomar and Hallock, 2008). Consistently, the microbial calcification was at optimum level during the Late Jurassic (Riding, 2000; Riding and Liang; 2005). In such a proximal nearshore setting, high nutrient input associated with terrigenous influx generally promote and increase calcareous algal production (Hallock, 2001). Subtle increase of nutrient input can result in modification of the benthic community environment ("phase shift" of Hallock, 2005) by limiting light penetration (Hallock, 2001) and rising the dasycline level (Alnazghah et al., 2013), causing disappearance of the shallow component community (e.g., dasyclads, oncoids, benthic forams). In the nearby sub-surface these facies have been interpreted by other workers as forming part of an internalite facies association representing a deep depositional setting (Al-Awwad and Pomar, 2015). Based on the stratigraphic position of the facies within the topmost part of the Jubaila sequence underneath the Arab evaporites, it is supposed that the facies may correspond to the regression and closing of the depositional system. The incorporation of the regional stratigraphic and paleogeographic position together with the associated sandstone suggests proximity to a detrital source and a relatively proximal setting.

F7: Bioturbated peloidal lime-mudstone to packstone: highly bioturbated lagoon

The facies are interpreted as low-energy protected lagoonal deposits. This low-energy environment was episodically disturbed by storm event responsible for the deposition of thin grainstone layers. The regional extent of these facies, the limited lateral facies changes and the dominant muddy carbonate texture are consistent with a shelf lagoonal depositional setting (Wilson and Jordan, 1983). The high faunal diversity, the abundant benthic forams and the associated ammonites and coral/stromatoporoids, the pale color of this facies and the intense bioturbation suggest a well-oxygenated environment and normal-marine salinites (Wilson and Jordan, 1983; Galli, 1993; Khetani and Read, 2002). The associated normal-marine fauna together with the regional stratigraphic positions suggest a distal lagoonal depositional environment.

F8: Sharp-based intraclast-peloidal skeletal grainstone, oncoidal locally: storm-dominated inner-platform

The erosional bed bases, graded bedding, and weak bioturbation suggest an instantaneous sediment accumulation (eventite) (Bádenas et al., 2012; Al-Awwad and Pomar, 2015). The plane-parallel lamination suggests high hydrodynamic energy, while the HCS and SCS (Fig. 8E) suggest sediment transport through oscillatory storm generated flows (Duke, 1985; Myrow and Southard, 1996; Morsilli and Pomar, 2012). These eventite beds were interpreted as a result of breaking of internal waves in the nearby subsurface Khurais Field (Al-Awwad and Pomar, 2015). It is unlikely that the internalites or pycnocline can exist or propagate in such epeiric flat-topped platforms (L. Pomar, personal communication). The depth of pycnocline (density stratified fluids) at such low latitude ranges from 600-1000 m to minimum 100 m at mid latitude (Morsilli and Pomar, 2012). It is doubtful that the turbulence of internal waves can transport or influence shallow-water components that are shallower than pycnocline level (Jacquemyn et al., 2017). The propagation of internal waves requires sufficient water depth on at least gently sloping ramp depositional profile (Bádenas et al., 2012). An alternative mechanism for transporting the conglomeratic rudstones of the Jubaila is debris or hyperconcentrated density flow related to offshore downslope directed flow

(Jacquemyn et al., 2017). Erosive channelized debris flows (such as Fig. 10) require relatively steep depositional slopes (> 4°, commonly >20°; Janson et al., 2011; Mullins and Cook 1986 in Jacquemyn et al., 2017). Steep clinoform geometries are not evident either on a regional outcrops cross-section (Fig. 5) or on a subsurface dip-direction cross-section (Fig. 14). Taking into account the paleogeographic setting, the regional succession with respect to the associated nearshore facies, a storm surge or coastal set up is suggested consistent with Jacquemyn et al. (2017). Wind-forced currents, promoted by a transgressive trend and increasing accommodation space, represent a possible mechanism for onshore sediment transport in such a flat depositional profile (cf. Aigner, 1985; Galli, 1993).

4.4 Barrier to back-barrier lagoon

F9: Oncoidal packstone, grainstone and rudstone: oncoidal bars/shoal

This facies formed in a high-energy shallow-marine sandy to pebbly bar or shoal depositional setting. The oncolites are valuable indicators for paleoenvironments as they are sensitive to turbidity- and trophic-levels, which, in turn, are controlled by climatic and relative sea-level changes (Védrine et al., 2007). Oncolites are interpreted to form preferentially in open-marine semi-arid settings (Védrine et al., 2007). The predominance of dasyclads (*Clypeina*), benthic forams and coral/stromatoporoid indicates shallow-marine, low-turbidity and optimum conditions for the carbonate factory.

F10: Coral/stromatoporoid boundstone to floatstone: low-energy and high-energy back-barrier

The circular patch-reefs and the coral/stromatoporoid biostromes are interpreted to have developed in a clear shallow and open-marine environment that was free of argillaceous matter (Védrine and Strasser, 2009). The paleogeographic and stratigraphic location of the reef biostromes and buildups suggest that these formed in a back-barrier depositional environment (Wilson and Jordan, 1983).

F11: Cross-bedded coated-grain and peloidal grainstone: shoal and washover complex

These facies were deposited in a high-energy depositional environment dominated by storm- and wave-generated currents. The stratigraphic position of this facies and spatial relationships with the other facies indicate a shoal and/or back-shoal washover environment (Reinson, 1979).

5 Sequence stratigraphy and stratigraphic evolution

The sequence stratigraphic transects are oriented N-S in an oblique direction to depositional dip (Fig. 4 and 5). The Upper Jurassic succession can be divided into two 2nd-order depositional sequences—the Hanifa sequence and Jubaila-Arab-D sequence. The basal sequence boundary of the Hanifa sequences corresponds to the Middle-Late Jurassic unconformity and is marked by sharp regionally extensive iron-stained hardgrounds associated with a slight truncation over the Tuwaiq Mountain Limestone. This unconformity corresponds to a 2nd-order sequence boundary (SB^2 11 of Al-Husseini et al., 2006).

The overall apparent depositional dip (proximal-distal polarity) is a northeast-southwest direction. The detrital siliciclastics increase toward the southwest, reflecting greater proximity to the terrigenous source and to the Arabian Shield (Fig. 13B; Ziegler, 2001). Relatively normal-marine facies and fauna increase toward the north and the northeast of the transects. These depositional sequences underwent evident differential subsidence and the location of the subsiding areas is different in each sequence. Therefore, subdivisions of these two depositional sequences were also based on their tectonically-related stratigraphy.

5.1 Hanifa Sequence Stratigraphy

The outcropping Hanifa Formation is composed of two third-order sequences (HCS1 to HCS2), each comprising multiple high-frequency sequences (HFSs). The HFSs show slight retrogradational and overall aggradational stacking patterns and lack well-developed progradational stacking patterns (Fig. 4). The lack of low-stand systems tract (LST) is attributed here to deposition in a flat-topped shelf inner-platform setting. The Hanifa Formation is dated Early Oxfordian to Early Kimmeridgian (Manivit et al., 1990). Therefore, the approximate duration of the Hanifa sequences is 5.3 Myr, and the average duration of the Hanifa composite sequences (HCS1-HCS2) is approximately 2.65 Myr.

5.1.1 Hanifa Composite Sequence 1 (HCS1)

5.1.1.1 HFS1

This high-frequency sequence is bounded by two subaerial exposure surfaces and marked by extensive stained bored hardground surfaces. It wedges-out in the Wadi Al Ain–Riyadh area. HFS1 consists of four cleaning upward cycles capped by coral/stromatoporoid boundstone (F10). These bioconstructed facies represent maximum transgression and highstand stage of the sequence.

5.1.1.2 HFS2, HFS3 and HFS4

High-frequency sequences HFS2-HFS4 are bounded by minor firmground and hardground surfaces and are characterized by an overall basal shallow-marine low-energy argillaceous deposits (F4 and F5) that are barren to low faunal diversity attributed here to proximity to siliciclastic and nutrient supply (Appendix 2 and 3). These proximal siliciclastic deposits are thickened and localized mainly in highly subsiding areas in which depressions seem to be compensated and filled with terrigenous sediment during initial transgression. The maximum marine transgressions of these sequences are marked by swaley cross-stratified grainstone (F11) in the southern-end section (Wadi Al Haddar) that are coincide with biostromal coral/stromatoporoid facies (F10) in the northern section (Huraimla). During the highstand systems tract (HST) of these sequences, the high-energy deposits evolved to lower energy highly bioturbated lime-mudstones (F7).

5.1.1.3 HFS5 and HFS6

These high-frequency sequences are characterized, at the base, by high-energy storm-generated grainstone deposits (F8) overlain by white-colored pure carbonate facies (F7 and F11). The storm-generated grainstones (F8; base HFS5) form an extensive correlatable layer within the study area. This layer was used as a lithostratigraphic marker separating the two Hanifa members—the Hawtah and Ulayyah Members (Vaslet et al., 1983). So, the lithostratigraphic boundary between the Hanifa members is a conformable transgressive surface within HCS1. There is no clear evidence of lateral facies-variation indicating a proximal-distal polarity in the overall strike transect, which is interpreted to represent a very extensive and shallow-marine inner-platform depositional setting. The lateral continuity and the tabular geometry of the storm generated meter-thick bedsets and the lack of clinoforms within the study area attest a very flat depositional profile. These extensive high-energy deposits imply significant sequence stratigraphic events in which the whole inner-platform became highly agitated. These higher-energy conditions are attributed here to an increase of accommodation space, resulting in greater propagation of waves and storms in inner-platform settings. Increased accommodation space is associated with normal-marine conditions during the Hanifa long-term transgression and backstepping trend. The synchronicity of normal-marine conditions and high-energy deposits (base HFS5) is testified by the high foraminiferal diversity (cf. Al-Mojel, 2017) including the first appearance of the Late Oxfordian benthic foraminifera *Alveosepta Jacardi* (Appendix 2 and 3). Remarkably, the first appearance of the *Alveosepta Jacardi* in the extensive grainstone deposits (base HFS5) is an important stratigraphic event. It was not recognized by a recent outcrop study (Fallatah and Kerans, 2018), which instead proposed diachronous clinoform geometries for this interval. The main MFS of HCS1 fits with the MFS of HFS5, which is locally characterized by swaley cross-stratified shoal grainstone (F11; Wadi Ghulghul) and biostromal coral/stromatoporoid (F10; As Sitarah).

HFS6 consists mainly of low-energy highly bioturbated wackestone/mudstone (F7) and local coral/stromatoporoid buildups (F10; Wadi Birk). The HFS6 is similar to the preceding cycle but the transgressive sharp-based grainstones (F8) and the swaley- and hummocky-stratified grainstones (F11) are thinner and less extensive, which is probably due to decreasing accommodation space. The HST of HFS6 is characterized by well-oxygenated highly-bioturbated (mainly *Thalassinoides*) mudstone/wackestone (F7) with locally coral/stromatoporoid buildups (F10). HFS6 is capped by a regional sequence boundary (top HCS1) marked by a stained bored hardground or an extensive ravinement surface. The top sequence boundary shows obvious facies shift from the clean low-energy carbonate-rich intervals to overlying brown and darker-color high-energy facies (F8). The top sequence boundary could be considered a slight tectonically-forced regional truncation surface (with probable subaerial exposure) in which the HST is notably thinning northward whereas the TST appears isopachous. The Wadi Birk–Riyadh area is slightly uplifted and eroded (less than 10 m compared with the southern area). Later on, this area seems to be slightly more subsiding at the beginning of the overlying HCS2 sequence as shown by its maximum thickness and thinning toward the south.

5.1.2 Hanifa Composite Sequence 2 (HCS2)

The sequence is made up of seven high-frequency sequences (HFS1-HFS7), each a few to ten meters thick and bounded by bored hard-grounds or transgressive ravinement surfaces. Most of these HFSs are more or less isopachous and can be correlated all along the transect. This broad tabular geometry and the facies distribution within these HFSs clearly show that the depositional profiles were uniformly regionally horizontal in this shallow-marine inner-platform environment. No clinoforms can be inferred from the geometries and facies distribution. The base of HCS2 (HFS1) is marked by an extensive transgressive bedset made up of decimeter thick storm-generated coarse-grained grainstone beds (F8), identified in all the sections except in Al Haddar to the south. Tidal influence is locally attested by bidirectional sigmoidal cross-bedding. Therefore, it is interpreted as a sandy shoreface-foreshore characterized by high-energy storm-dominated ravinement processes in a transgressive context. These early-transgressive grainy bedsets (F8) are overlain by low-energy bioturbated slightly argillaceous muddy carbonate deposits (F4; HFS2). The lower part of HCS2 (HFS1 and HFS2) shows limited lateral facies variations and the shale content increases toward the south (Al Haddar) and toward the proximal domain, which supports the continental origin of the shale influx and its interpretation as a proximality indicator. In the upper part of HCS2 (HFS3-HFS7), the facies distribution is much more complex and dominated by the widespread development of coral/stromatoporoid boundstones (F10) and associated oncoidal grainstones (F9) with minor low-energy muddy intervals (F7). These facies indicate rapid facies variations at a hectometric to kilometric scale resulting in a very complex architecture of the upper part of the HCS2 and of related potential reservoir bodies in this interval. The general migration/backstepping of the corals/stromatoporoids bodies (F10) southward confirms the overall TST of HCS2. The MFS of HCS2 (MFS of HFS6) is marked by the maximum southward (landward) extent of the highly-bioturbated lagoonal peloidal mudstone/wackestone facies (F7); and in the north it is marked by the most distal facies of the swaley cross-bedded peloidal shoal grainstones (F11). This MFS represents the main maximum transgression of the whole Hanifa sequence. Interestingly, the lateral southward facies changes (Fig. 11B; T4) from normal-marine reefs (F10) to algal microbial system (F9) is probably controlled by the proximality to terrigenous sources and an associated nutrification input. The increasing of nutrient supply could switch the carbonate production from reef to algal depositional system (cf. Fig. 9 in Hallock, 2001). The highstand systems tract (upper HFS6 and HFS7) lacks argillaceous detrital content suggesting that shorelines were pushed further updip during continuing coastal onlap of MFS and HST units. The top Hanifa sequence boundary is a disconformity marked by an extensive iron-stained hardground surface, which was considered as a third-order sequence boundary (SB^3 11.3 of Al-Husseini et al., 2006), but herein is interpreted as 2nd-order sequence boundary. This erosional surface is associated with abrupt facies changes as it separates coral/stromatoporoid prone facies at topmost Hanifa Formation from storm-influenced darker-color quartz-rich grainstones at the base of the Jubaila Limestone. Therefore, it is possible that the regressive systems tract of HCS2 may have been partially eroded. Our correlations show also a slight differential uplift of the southern area where truncation is most pronounced. It is abruptly overlain by the top Hanifa exposure and base-Jubaila ravinement surface with a very limited preserved highstand systems tract.

5.2 Jubaila and Arab-D Sequence Stratigraphy

The facies distribution of the Jubaila-Arab-D outcrops indicate conformable genetically-related successions comprising two third-order sequences (JCS1 and JCS2). The lithostratigraphic boundary between the Jubaila Limestone and the Arab Formation (*sensu* Manivit et al., 1991; Appendix 1) seems to be a conformable surface within JCS2 (Fig. 5). The Arab-D anhydrite, located in the upper part of the Arab-D Member, is not part of the Jubaila-Arab-D sequences because the thickness of the evaporites increases upward, which implies an increase in accommodation space attributed here to the TST of the next sequence. In the subsurface, the Arab-D reservoir has been divided into three informal time-stratigraphic zones based on porosity log correlation (Mitchell et al., 1988). These reservoir zones are extended to the outcrops sections through subsurface correlation with Khurais and Ghawar fields (Fig. 14).

The Jubaila-Arab-D sequences are dominated by a carbonate deposition with subordinate siliciclastics (mainly quartz sandstone, no argillaceous sediments). The Jubaila-Arab-D sequences formed in an overall low-energy wide lagoon on a flat-topped inner-platform subjected to transgressive-related storm pulses. The stacking patterns lack well developed progradational geometries and low-stand systems tract (LST) in the studied outcrop.

An early Kimmeridgian age attribution for both the upper Hanifa sequence (HCS2) and lower Jubaila Limestone (JCS1), suggests that upper Jubaila and Arab-D Member (JCS2) may extend into the late Kimmeridgian. Therefore, the approximate duration of the Jubaila-Arab-D sequences could be ~ 4 Myr, with the average duration of the two composite sequences (JCS1 and JCS2) being approximately 2 Myr.

5.2.1 Jubaila and Arab-D Composite Sequence 1 (JCS1)

JCS1 consists of two high-frequency sequences (HFS1 and HFS2). HFS1 shows wedging geometry and increasing thickness toward the central part of the studied area (Wadi Al Ain). This is attributed to a progressive synsedimentary differential subsidence increasing eastward (Fig. 5). The base of the HFS1 is characterized by storm transgressive grainstones and floatstone/rudstone (F8) with rip-up clasts and around 30% sandstone quartz. They are interbedded with barren thinly laminated lime-mudstone (F6) and weakly bioturbated nodular wackestone with low foraminiferal species diversity (*Nautiloculina oolithica* and *Lenticulina* sp.) corresponding to a proximal restricted lagoon facies association. The storm beds formed aggraded, extensive, and correlatable units, which imply a near-horizontal bathymetric profile after the top Hanifa exposure. The depositional profile remained very flat during the synsedimentary deformation as suggested by the lack of lateral facies variations. Coral/stromatoporoid facies are notably absent in the HFS1. The MFS of HFS1 is placed within thickest storm grainstone bed in the most proximal section (Al Haddar). This is because development of wave and storm dynamic and propagation require a higher accommodation space in such a wide lagoon. The HST of HFS1 is marked by a progressive upward thinning of the storm grainstone beds (F8) that grade upward to highly bioturbated lagoonal mudstone/wackestone (F7) which is rich in benthic foraminifera. During the highstand, waves and storms became fetch-limited due to either the unique physiography of the Arabian Platform and the great distance of the studied area from the ocean or due to the establishment of shoals and reefs in outer barriers (e.g., shelf margin). The lagoonal muddy facies (F7) are aggrading and still in connection to the ocean and open-marine influence as indicated by strong bioturbation and the migration of the pelagic fauna (ammonite and nautiloids) into this proximal setting. Through the HST, the intensity of the bioturbation of the lagoonal facies (F7) decreases progressively upward, culminating in barren thinly laminated lime-mudstone (F6; Appendix 4), which imply an increase in restriction and protection upward. The restriction is probably caused by a short-term regression and seaward stepping of nutrient input. The top sequence boundary of the HFS1 is not clearly defined but it can be placed at the maximum northward extent of restricted lagoon facies (F6).

HFS2 is tabular and exhibits no lateral thickness variations. The TST is marked by a progressive upward thickening of the storm grainstone beds (F8) and increased abundance of the bioturbated wackestone/packstone facies (F7), which imply more marine influence and decrease of the nutrient supply. The bioturbated wackestone/packstone facies (F7) shows a slight retrogradational stacking-pattern toward the proximal domain to the south. The storm grainstones (F8) are quartz-rich and dominated with oncoid and coated-grains floatstone/rudstone. Very rare reworked clasts of coral/stromatoporoids were noticed in these grainstone beds. Through the transgression trend, the upward change from barren restricted lime-mudstone (F6) to more algal microbial system is related to the decrease in nutrient influence (cf. Hallock, 2001). The lagoonal facies tract remained partially restricted and was not fully marine as indicated by low faunal diversity and poorly developed reefal facies (F10). The MFS of HFS2 is picked at the maximum back-step of bioturbated lagoonal facies (F7) toward the proximal domain found to the south. In the TST of HFS2, there is a clear synchronicity between depositional energy, faunal diversity and bioturbation. The very-low energy facies (F6) is barren and not bioturbated but when it grades to wackestone/packstone (F7) storms and faunal diversity become apparent (Appendix 4). On this flat-topped platform, depositional energy and the degree of protection seem to be related to the paleogeography or physiography of the Arabian Platform rather than a water depth relationship. The HST is marked by an upward thinning and decrease in storm grainstone facies. The vertical facies proportion of the storm grainstones through HFS2 suggest that storms are cyclic and transgressive in origin. The top sequence boundary (top JCS1) is probably a subaerial exposure marked by regionally extensive red dolomite beds (F2) with local silicified evaporite nodules (Wadi Al Haddar), which are attributed to a restricted tidal or salina recharge process. This sequence boundary (top JCS1) has been recognized by numerous previous studies (Powers, 1962; Mitchell et al, 1988; Meyer and Price 1993; Handford et al., 2002; Lindsay et al., 2006; Al-Awwad and Collins, 2013b).

5.2.2 Jubaila and Arab-D Composite Sequence 2 (JCS2)

The JCS2 consists of three high-frequency sequences (HFS1-HFS3). HFS1 thins slightly to the north as a result of syndepositional differential subsidence. The TST shows a progressive upward decrease in quartz content. The MFS is marked in the distal domain (Wadi Malham) by high-energy grainstones (F8) with erosional base and associated with coral/stromatoporoid buildups (F10) and reworked clasts (Fig. 10). In this inner-platform setting, the coral/stromatoporoid system is widely influenced by wave and storm dynamic. The waves and storms are really the dominant factor during maximum marine transgression of the Jubaila deposition. In several previous interpretation, these reef buildups have been considered to represent highstand prograding fringing reefs (Lindsay et al., 2006; Al-Awwad and Collins, 2013b). The reef facies (F10) have to be interpreted as back-barrier backstepping units and not classic prograding units, as indicated by disappearance of these facies in the proximal domain of the transects (Wadi Al-Haddar). The HST of HFS1 is marked by progressive finning upward and minor regression and seaward stepping of the barren lime-mudstone (F6).

HFS2 thins slightly to the north. During the TST, the quartz content decreased upward and the depositional system becomes high-energy dominant with an open-marine fauna of coral/stromatoporoid and rudist floatstones/rudstones (F10; Wadi Malham, Al-Hawtah). The MFS of HFS2 is placed in the maximum landward extension of the coral/stromatoporoid and rudist floatstone/rudstone (F10) to the south indicating a well-circulated normal-marine back-barrier lagoon. Through the HST of HFS2, the coral/stromatoporoid facies (F10) grades progressively upward to oncoid and coated-grains floatstone/rudstone (F8) accompanied by an increase in quartz content and thickening of quartz-rich red dolomite beds (F2; Wadi Malham). This vertical change from a reef dominated depositional system to a more algal microbial system is attributed to increased nutrient influence (cf. Hallock, 2001) through the regression trend. The top sequence boundary of HFS2 is marked by a quartz-rich red dolomite bed (F2; Wadi Malham).

The HFS3 has tabular geometry and no lateral thickness variations, and is characterized by barren lime-mudstone (F6) and bioturbated wackestone facies (F7), while normal-marine coral/stromatoporoid facies (F10) are notably absent. The HST is marked by a slight northward progradation of restricted low-energy lime-mudstone (F6). The top sequence boundary (top JCS2 and whole Jubaila-Arab-D cycle) is marked by an erosional ravinement surface overlain by dolomitized grainstones (F8) with reworked silicified evaporite nodules (Wadi Malham) and local hummocky cross-stratification (Al Hawtah). The grainstones are overlain by anhydrite dissolution residue and rotated rafts of stromatolitic dolomite.

6 Discussion

6.1 Evolution of depositional systems

6.1.1 Hanifa Formation

The Hanifa Formation has been previously interpreted as two composite sequences—the Hawtah sequence and Ulayyah sequence (Sharland et al., 2001; Mattner and Al-Husseini 2002; Al-Husseini et al., 2006; Hughes et al., 2008; Hughes 2009; Le Nindre in Kadar et al., 2015). The first sequence, defined herein (HCS1), is broadly equivalent to the Hawtah sequence, while HCS2 would be equivalent to Ulayyah sequence.

The main MFS of the HCS1 is placed here within the Late Oxfordian backstepping of high-energy deposits, coincident with the highest faunal diversity (Appendix 2 and 3). Conversely, other workers placed the MFS of the Hawtah sequences in the Middle Oxfordian (*plicatilis* Zone) (MFS J50 of Sharland et al., 2001; Mattner and Al-Husseini, 2002; Le Nindre in Kadar et al., 2015). Alternatively, Hughes et al. (2008) placed the MFS's in argillaceous limestone with the highest gamma-ray signals (Appendix 2). They interpreted the argillaceous limestone interval as deep-lagoon environment based on associations of micro- and nanofossils. Similarly, Al-Mojel and Kerans (2014) and Fallatah and Kerans (2018) placed the Hanifa MFS in an argillaceous limestone interval interpreted as offshore deposits based on lithology, stressed low-oxygenation conditions and low bioturbation levels. The elevated argillaceous content at the base of the sequences is interpreted here not as a sign of deepening given the shallow flat inner-platform setting, but rather as an indicator of an initial transgression over nearshore siliciclastics. The MFS is placed higher in a regionally extensive limestone with cleaning gamma-ray trend as it shows onlapping with widespread corals/stromatoporoids facies and the invasion of ammonites onto the shelf. In this scenario siliciclastics backstep updip during the MFS and HST. In contrast to classical interpretation, MFS and HST are characterized by a cleaning-upward gamma-ray trend.

6.1.2 Jubaila-Arab-D

The sequence stratigraphy of the Jubaila Limestone and Arab-D reservoir has been the subjected of many-detailed outcrop and subsurface studies (e.g., Powers, 1962; Mitchell et al., 1988; Le Nindre et al., 1990; Meyer and Price, 1993; Handford et al., 2002; Lindsey et al., 2006; Al-Awwad and Collins, 2013a, 2013b; Al-Awwad and Pomar, 2015; Jacquemyn et al., 2017). The sedimentological description in most of these previous studies was limited to the so-called “Arab-D reservoir,” which corresponds to the upper part of the Jubaila Limestone and Arab-D Member (HFS2 of JCS1 to JCS2). The previous studies are lacking a wider regional sequence stratigraphic cross-section documenting lateral facies changes of the Jubaila Limestone and base Arab-D reservoir. These lateral facies changes are less evident in the subsurface and specifically across the Ghawar field, 300 km west of Riyadh (Mitchell et al., 1988). In some of these previous studies, the barren lime-mudstones (F6) are interpreted as having been deposited in a distal ramp depositional setting (e.g., Handford et al., 2002; Lindsay et al. 2006; Al-Awwad and Collins, 2013b; Al-Awwad and Pomar, 2015). Alternatively, Powers (1962) and Mitchell et al. (1988) considered the barren lime-mudstones (F6) of Zone 3 and lower Zone 2 as representing deposition in a restricted, very shallow and quiet water environment.

The reasoning behind previous interpretation of the lime mudstone (F6) as distal facies is that low energy and poor light penetration are interpreted to be associated with a deepwater setting (Al-Awwad and Collins, 2013b). These two conditions (low-energy and poor light-penetration) could also prevail in a sheltered or protected shallow-marine carbonate system on this exceptional extensive platform (Fig. 13B). High coastal nutrient input from surface run-off could limit light penetration (Hallock, 2001) and cause restricted low-oxygenated conditions controlled by density stratification that prevented vertical circulation of bottom water (Bottjer et al., 1986; Rabalais et al., 1991; Lukasik et al., 2000). These factors could result in a distinct change in the environment of benthic communities, a “phase shift” according to Hallock (2005). This would explain the disappearance of some of the biological community (e.g., dasyclads, oncoids, benthic forams). Having the barren lime-mudstones (F6) deposited in a proximal nearshore setting with high coastal-nutrient input is consistent with the associated high-content of quartz sandstone in outcrop and in the subsurface (Fig. 14; Zone3, Lindsay et al., 2006). The updip equivalents of these restricted lime-mudstones (F6) are the coastal quartz sandstones and conglomerates (Fig. 5; Wadi Al Majami, Vaslet et al., 1985). Other evidence supporting the interpretation adopted herein is that similar barren lime-mudstones (F6) occur higher in the Arab-D reservoir directly underneath the intertidal facies (Zone1) and anhydrites, in both outcrop (Fig. 5) and subsurface (Al-Awwad and Collins, 2013b). Modern example of continental shelf that undergoes eutrophication and hypoxic bottom-waters can be found near the discharge of the Atchafalaya and Mississippian Rivers in the northern Gulf of Mexico (Turner and Rabalais, 1994; Rabalais et al., 2002). This inner-continental shelf represents the largest oxygen-depleted zone in the Western Atlantic (Rabaiais et al., 1991; Boesch and Rabalais, 1991, in Turner and Rabalais, 1994). Several modern analogs were presented by Hallock and Schlager (1986) that show negative influence of nutrients on carbonate platforms.

Interpreting lime mudstones as basinal or outer-ramp deposits has lead the previous authors to propose a slope-related depositional model that has led to a shallowing upward paradigm for the interpretation of the Jubaila-Arab-D sequence (Meyer and Price, 1993; Handford et al., 2002; Al-Awwad and Collins, 2013b; Al-Awwad and Pomar, 2015). These interpretations contradict the extensive correlatable layer-cake stratigraphic architecture observed in the outcrop and in the subsurface (Fig. 13; HFS2 of JCS1; Figure 15 of Mitchell et al., 1988; Meyer and Price 1993). The layer-cake sequence stratigraphic framework of the Jubaila-Arab-D presented here (Fig. 5 and 13) are consistent with the interpretation of Wilson (1975), Murris (1980) and Mitchell et al. (1988) showing similar tabular geometries. An inclined topography (the clinoform ramp model) requires progradation toward the thickest part of Jubaila-Arab-D sequence to fill the accommodation space (Al-Awwad and Collins, 2013b). This interpretation contradicts the evidence for syndepositional differential subsidence playing a significant role in the thickness variations of the Jubaila Limestone (e.g., HFS1 of JCS1).

6.1.3 Evolution of carbonate system in a transgressive inner-platform

The studied outcrops are located on the proximal part of a very wide epeiric platform, more than 1000 km from the platform margin (Fig. 13B). There are no really deep-marine facies associations observed in the studied interval. The depositional system is characterized by an association of low-energy muddy deposits, sometimes slightly argillaceous, and high-energy grainstone with occasional sandstones. The sedimentary structures of these high-energy deposits suggest an origin of storm-related currents. Following a ramp depositional model, the storm deposits were previously interpreted as having formed in upper offshore deposits (e.g., Lindsey et al., 2006; Al-Awwad and Collins, 2013a, 2013b; Al-Awwad and Pomar, 2015; Jacquemyn et al., 2017). The sediments do not show the classical characteristics of such environments, such as fine-grained sediments with well-developed HCS structures. Offshore lower-shoreface storm deposits tend to be narrow and localized belts and more often show prograded lenticular grainstone bodies. Instead, these storm-generated grainstones are extensive, regionally continuous and correlatable suggesting an overall synchronous deposition in a flat-topped inner-platform setting. Most of the high-energy depositional units have a sharp-based contact with the underlying muddy deposits. A gradual coarsening-up evolution, which should exist in a prograding system, has never been observed in the studied sections. The sharp-based surfaces are interpreted as ravinement surfaces related to transgressive processes and not to sea level drops or associated forced-regressive processes. The transgressive ravinement surfaces are extensive and considered as timelines. Considering the overall context, the low-energy deposits are unlikely to be deeper offshore facies but rather inner-platform lagoonal facies.

The Hanifa and Jubaila stratigraphic transects exhibit a very tabular geometry and wide lateral continuity. The only clinoforms that have been identified by seismic reflections in the subsurface are located more to the east (Fig. 13; Keho et al., 2009) and are related to the development of an intrashelf basin (see discussion below). In this type of platform-intrashelf basin system, the deeper environments are in contrast to the barren lime-mudstone (F6) characterized by organic-rich lime-mudstones (cf. Droste, 1990; McGuire et al., 1993; Al-Naji, 2002; McGuire, 2003) that have not been observed in the outcrop area (Fig. 13).

6.1.4 Insights into the development of the Late Jurassic intrashelf Arabian Basin

Surface-to-subsurface correlations (Fig. 13 and 14) provide insight into the development and evolution of the Upper Jurassic intrashelf Arabian Basin. Paleogeographically, the intrashelf Arabian Basin is more than 500 km landward from the Neo-Tethys continental margin (Fig. 13B; Murris, 1980; Ziegler, 2001). To the north, the intrashelf basin is bounded by broad Rimthan Arch which is characterized by shallow-marine peritidal deposits and exposed islands (Mattner and Al-Husseini 2002; Ziegler, 2001). To the east the intrashelf basin is bounded by the Qatar Arch (Murris, 1980), while it is limited to the west (Khurais to outcrop) by a flat-topped carbonate platform with a margin located near Khurais field (Fig. 13). A basinal intrashelf source rock is characterized by laminated dark organic-rich lime-mudstone facies (McGuire et al., 1993; Al-Naji, 2002). The Hanifa reservoir facies are characterized by oolitic and peloidal shoal grainstones and some coral/stromatoporoid floatstone located, in the cross-section (Fig. 13), only in the southern Rimthan Arch and in the Khurais Field. Within the central Arabian Basin (North Ghawar and Qatif), the Hanifa Formation comprises a non-reservoir thick lime-mudstone interval (McGuire et al., 1993; Al-Naji, 2002). The shoal grainstones in the southern Rimthan Arch formed on a gentle ramp that dips southward at < 0.5° (McGuire et al., 1993; Al-Naji, 2002). The shoal grainstones in the Khurais Field are aggrading and characterized by limited migrations (Keho et al., 2009). These high-energy reservoir facies seem to correlate with the outcropping high-energy open-marine carbonate facies of HCS1 and HCS2. They most likely formed during maximum accommodation space that allowed open-marine conditions and wave energy to propagate inboard in such extensive protected flat platform. In addition, the high rate of accommodation space resulted in a differential aggradational style on the platform as carbonate production is not able to fill up the created space everywhere (cf. Ayres et al., 1982; Razin et al., 2010, 2017). High carbonate productions that follow the rapid accommodation rate were localized in certain places forming aggrading stacking patterns, as in Khurais and in the southern Rimthan Arch. While sedimentation in the central Arabian Basin lagged behind causing the creation of intrashelf basin with about ~70 m water depth (estimated by reconstructing depositional profile from one of the Hanifa cycles in Fig. 13). Accordingly, in this interpretation the formation of the deep intrashelf basin and the subsequent infill with source rock is synchronous with the transgressive high-energy shallow-marine deposits. The high productive and high-energy areas do not seem to prograde much to fill the intrashelf basin during HST. During the highstand sea-level phase, depth of wave-base seems to decrease due to waved dissipation and distraction promoted by the remoteness of the basin from the ocean and probably by the growth of carbonate outershelf barriers. Therefore, protected and perhaps restricted lagoonal carbonate mud would drape and infill the topographic low during HST, which is consistent with seismically mapped draping geometries at scale of the basin by (Keho et al., 2009).

The Jubaila-Arab-D sequence seems to be flat-topped homogeneously aggrading platform succession with no deep intrashelf basin. The Jubaila Limestone overlies the Hanifa Formation with lowstand deposits (Hanford et al., 2002) that appear to be localized west of the Khurais field. The top Hanifa disconformity (from Khurais toward outcrop) seems to be an onlapping surface. The shallow carbonate platform aggraded and kept up as a response to this continuous and slight syndepositional differential subsidence (cf. Wilson and Jordan, 1983), resulting in lateral thickness variations as well as slight lateral facies changes. The syndepositional differential subsidence decreased upward and more uniform subsidence prevailed in the Arab-D reservoir in which JCS2 shows tabular geometries (Fig. 14).

6.1.5 Progradation direction of the Arab-D

Figure 14 shows a sedimentological-based regional sequence stratigraphic correlation of the Arab-D across the Arabian Basin. The Arab-D in the southern Rimthan Arch (JCS2) is characterized by an overall high-energy shoal facies overlain by domed coral-stromatoporoid rudstone facies. The shoal facies migrated inboard to the south on a very low-angle (<1°) ramp profile with 0-12 m water depth. Depositional cycles were capped by exposure surfaces evidenced by dense dolomite and anhydrite beds with crinkly lamination, mud crack and desiccation features. Meteoric cements (pendant and meniscus) were noticed below the cycle boundaries. In the central Arabian Basin (Khurais and North Ghawar), the facies of the Arab-D (Zone 4 and 3) is characterized by micritic to very fine-grained sediments capped by firmgrounds and hardgrounds interbedded with storm-derived rudstone and floatstone (Fig. 14; Al-Awwad and Collins, 2013a; Lindsay et al., 2006). Arab-D (Zone 2) is characterized by domed, encrusted and branched coral/stromatoporoid packstone and floatstone with some ooid grainstone overlain by dasyclad, encrusting algae wackestone/packstone and *Cladocoropsis* rudstone and floatstone (Al-Awwad and Collins, 2013a; Lindsay et al., 2006). The succession of the Arab-D is partitioned by occasional sheet-like dolomite beds with fabric- and nonfabric-preserving texture. The dolomites have been interpreted as have formed syndepositionally, from hypersaline fluids derived from overlying salina (Lindsay et al., 2006). The regionally extensive dolomite appears to be stratigraphically related to tidal recharge/infiltration and seepage-refluxion processes (Adams and Rhodes 1960; McKenzie et al., 1980; Enos, 1983; Lannace and Frisia, 1994). The long-term climate changes, with increasing cooling and aridity, during Late Jurassic have an influence on the dolomite distributions. The formation of these extensive sheet-like dolomites across the Arabian Basin seems to be controlled by low accommodation rates. The rationale behind this Arab-D sequence stratigraphic framework (Fig. 14) is that the sheet-like dolomites represent essentially synchronous stratigraphic events in which inner-platform and intrashelf basin being restricted and highly evaporated during relative sea-level fall (late-HST/LST). The dolomites occur preferentially around sequence boundaries and are rare or absent in maximum flooding intervals with a backstepping of normal-marine high-energy facies (e.g., coral/stromatoporoid).

The long-term evolution of the Jubaila and Arab-D depositional system can be divided into sequential depositional model with 5 time steps (Fig. 15). During early transgression, the platform probably lacked a barrier system and was subjected to transgressive high-energy storm pulses, which brought relative normal-marine conditions and pelagic fauna into the proximal inner platform (Fig. 15A). This resulted in intercalation of extensive restricted barren lagoonal lime-mudstone and storm-grainstone beds (JCS1; Fig. 15B). During maximum marine transgression (MFS of JCS2), a backstepping of normal-marine and higher energy conditions are responsible for development of shoal grainstones across paleohighs and extensive back-barrier reef facies (Fig. 15C). During the HST of JCS2, reef facies prograded out from the intrashelf basin toward the Rimthan Arch leaving behind an aggradational extensive clear lagoon with dasyclad, encrusting algae and *Cladocoropsis* wackestone to packstone facies (Fig. 15D). During late HST (topmost JCS2), the platform was limited to no accommodation space during which time the inner-platform (outcrop) was probably exposed and restricted tidal flats developed within the intrashelf basin (Fig. 15E).

6.2 Controlling factors of the Oxfordian and Kimmeridgian stratigraphy

6.2.1 Tectonics and subsidence rates

The onset of the Oxfordian is marked by a shift in depocenter location and reversed dip-direction compared with the preceding Early and Middle Jurassic successions (early-Toarcian to middle-Callovian; Al-Mojel, 2017). The Oxfordian depocenter axis shifted to the south (As Sitarah section). This changes in basin configuration is probable related to a significant tectonic uplift and truncational event at the post-Tuwaiq unconformity throughout eastern Arabia (Iran, Abu Dhabi and Interior Oman; Gollesstaneh, 1965; Al-Suwaidi and Aziz, 2002; Rousseau et al., 2006). This erosional surface is responsible for the truncation of 200 m of carbonate deposits in eastern Interior Oman (Rousseau et al., 2006). This end-Tuwaiq truncation has also been noticed in the central Arabian Platform in the Rub' al-Khali Basin and in the northern part of the Ghawar field in what is called the “pre-Hanifa unconformity” (Powers, 1968). This tectonic instability is probably related to the incipient breaking of the Arabian-Indian plate boundary (Ziegler, 2001). There is another shift in depocenter and a reversal of onlap direction during the Late Oxfordian Early Kimmeridgian sequences (between HCS1 and HCS2). This reverse in polarity has been documented in the subsurface and is supported by seismically based stratigraphic sections and in a gamma-ray cross-section (Langdon and Malecek, 1987). Therefore, this sequence boundary is a critical surface that has to be considered for reservoir studies and regional exploration. Oxfordian tectonic interruptions were noticed in other Tethyan regions. For example, the Jura Platform in the northern margin of the Tethys Ocean had discontinuous subsidence history and wobbling blocks movement during the Oxfordian (Strasser et al., 2015). Syndepositional tectonic activities have been documented in Tunisia (Walley, 1985) and in NW Tethys in central Europe (Dardeau et al., 1988; Lhamyani, 1985; Pittet and Strasser, 1998; Allenbach, 2001; Chevalier et al., 2001; Védrine and Strasser, 2009; Strasser et al., 2015). In particular, Late Oxfordian (late *bifurcatus* Zone) inversion in the Swiss Jura Mountains (Allenbach, 2001, 2002) could be synchronous with the tectonic event noticed herein (between HCS1 and HCS2).

Figure (13) demonstrates the evolution of the Arabian Intrashelf basin. The Hanifa sequence is almost isopachous in the intrashelf basin, suggesting negligible differential subsidence. Differential subsidence is unlikely to be the main control on the development of the deep source-rock intrashelf basin, which is instead influenced by the changing ratio of carbonate production and accommodation space (see discussion above). Significant syndepositional differential subsidence occurs during the lower half of the Jubaila-Arab-D sequence with an abrupt thinning toward the Rimthan Arch. This is consistent with an overall eastward thinning of the Upper Jurassic stratigraphy toward the shelf margin as recorded by (Murris, 1980; Abu-Ali and Littke, 2005). Limited subsidence of the shelf margin and Rimthan Arch is probably the main reason for the lower Jubaila sequence being restricted and protected from open marine influence.

6.2.2 Eustatic control

The basal sequence boundary of the Hanifa sequence corresponds to an extensive regional unconformity with an Early Oxfordian (*mariae* Zone) hiatus

(Le Nindre in Kadar et al., 2015). This sequence boundary is one of the regional emersion and disconformity surfaces in the Jurassic of the central Arabia that is marked by major negative $\delta^{18}O$ excursions reported below sequence boundaries (Al-Mojel et al., 2018). This unconformity most likely resulted from a substantial eustatic sea-level fall (Haq, 2018) superimposed on local tectonic uplift and easterly uplift of the Arabian Platform (Ziegler, 2001). This Middle-Late Jurassic global sea-level fall could be glacio-eustatic in origin as it corresponds to a Late Callovian (*lamberti* Zone) maximum cooling event (Hallam, 1988; Dromart et al., 2003a, 2003b; Nunn et al., 2009; Nunn and Price, 2010; Donnadieu et al., 2011; Pellenard et al., 2014). This drop in sea level has been recorded in the relative sea-level curve of the Arabian Platform with around 40 m sea-level fall (Haq and Al-Qahtani, 2005).

The main MFS of the Hawtah sequence (HCS1) is dated from the Late Oxfordian based on the first occurrence of the foraminifer *Alveosepta jaccardi* and placed within a remarkably constant carbonate grainstone package. The appearance of the *A. jaccardi* may extend slightly below the widespread grainstone (Hawtah-Ulayyah boundary) as it appears to be the case in two outcrop sections (in Manivit et al., 1990). Although *A. jaccardi* is generally given a Late Oxfordian-Kimmeridgian range, some occurrences are considered as Middle Oxfordian (Bassoulet and Poisson, 1975, Hardenbol et al., 1998). Note that the late Middle Oxfordian *transversarium* Zone, which is not demonstrated in the Hanifa, would represent the transition between *Euaspidoceras* beds and the *A. jaccardi* beds (Fig. 16). The MFS J50 of the Arabian Platform would be better placed in the Late Oxfordian instead of the Middle or Early Oxfordian as in previous studies (Sharland et al., 2001; Mattner and Al-Husseini, 2002; Hughes et al., 2008; Le Nindre in Kadar et al., 2015). This Late Oxfordian MFS J50 coincides with a positive $\delta^{13}C$ peak, which has been interpreted as a sign of important marine productivity level favored by a high sea-level (Al-Mojel et al., 2018). The Late Oxfordian MFS is consistent with the Gulf of Mexico major marine transgression (Mancini et al., 2004) and with the Central North Sea (Carruthers et al., 1996). The major MFS in the Western Europe occurs in the Early Oxfordian (Hardenbol et al., 1998). This discrepancy in the global MFS suggests a local tectonic overprint on the eustatic signal of the Oxfordian. As argued here, a major sequence boundary and disconformity between HCS1 and HCS2 is most likely to be Late Oxfordian in age. This sequence boundary could correlate with the Western Europe 2^{nd}-order regression and sequence boundary between OX6 and OX7 (Fig. 16; Hardenbol et al., 1998; Strasser et al., 2000; Védrine and Strasser, 2009) and corresponds to JOx6 sequence boundary of Haq (2018).

The MFS of the Ulayyah sequence (HCS2) would correspond to the Early Kimmeridgian MFS J60 of Sharland et al. (2001). The precise placing of MFS J60 is debated and it has been suggested that the MFS J60 can be in the Lower Kimmeridgian either in Upper Hanifa (Ulayyah Member) or lower Jubaila (J1 unit; R. B. Davis in Kaddar et al., 2015). In this study we place the MFS J60 in the upper Hanifa (HCS2) instead of the Lower Jubaila, which is characterized by a lowstand and restricted lagoonal deposits (Fig. 13; cf. Handford et al., 2002). This lower Kimmeridgian MFS J60 could be synchronous with the precisely dated ammonite-bearing “coal horizon” of the northern Gotnia Basin, which yields *Orthosphinctes desmoides* (mid *platynota*

Zone, *desmoides* Subzone; cf. Howarth, 1992) and with a correlative horizon yielding abundant specimens of the ammonite *Ardescia enayi* (mid *platynota* Zone, *desmoides* Subzone) within the basal rift successions of southern Yemen (Toland, unpublished). Interestingly, the link between long-term transgression and reef expansion is characteristic of the Upper Jurassic elsewhere also, as noticed by Pittet and Strasser (1998) (e.g., Leinfelder 1993, 1994; Keupp et al., 1993). The Lower Jubaila restricted lagoonal deposits are considered herein as initial transgression, whereas topmost upper Jubaila (JCS2; Arab-D) records the maximum marine transgression with high-faunal diversity and backstepping of reef facies. This Jubaila-Arab-D MFS would correspond to the Upper Kimmeridgian MFS J70 (Sharland et al., 2001; Le Nindre in Kadar et al., 2015). This is consistent with Kadar et al. (2015) interpretation that placed MFS J70 in a clean limestone within the topmost Jubaila, just underneath the Gotnia Anhydrite in Kuwait. This Jubaila-Arab-D long-term transgression is in concordance with a global rise in eustasy (Haq, 2018) and the 2nd-order TST and MFS in the central Swiss Jura as well as in most of the Western European basins, which is placed in the Late Kimmeridgian (*eudoxus* Zone) (Hardenbol, 1998; Colombié and Strasser, 2005). These Swiss Jura large-scale sequences are correlatable in most of Western European basins, suggesting a strong eustatic influence on the Kimmeridgian sequences (Colombié and Strasser, 2005).

7 Conclusion

The Upper Jurassic outcrops formed on a broad slowly subsiding epeiric tropical platform. The depositional environment ranges from semi-arid shoreline to carbonate inner- and back-barrier lagoon, representing an aggraded flat-topped platform. Syndepositional differential subsidence influenced lateral thickness variation and to a lesser extent facies distribution. The Upper Jurassic successions consist of two 2nd-order sequences (Hanifa and Jubaila-Arab-D) superimposed by several 3rd-order composite sequences interrupted momentarily by short emersion sequence boundaries. The Hanifa Platform is mud-dominated and evolved from proximal argillaceous-limestone with low-faunal diversity to back-barrier open-marine carbonate platforms with reef bearing and high-faunal diversity. The deep intrashelf basin in the adjacent subsurface is associated with local low-angle clinoforms formed as a response to differential carbonate sedimentation during maximum marine transgression. The Hanifa Formation has two main MFS's placed in terrigenous-free carbonate sediments at the Late Oxfordian and Early Kimmeridgian. The Jubaila-Arab-D is consisting of two composite sequences that show long-term transgression marked at the base by storm-influenced inner-platform deposits and proximal barren lime-mudstone. The maximum marine transgression is placed in the Arab-D reservoir (Upper Kimmeridgian) in a backstepping of back-barrier high-energy reef facies. During the highstand, the reef facies gently prograded toward the Rimthan Arch leaving behind restricted lagoon and sabkhah/salina anhydrite. These Upper Jurassic sequences are probably controlled by eustatic factors, coupled with local tectonic disruption, as they have some similarity with other Tethyan sequence stratigraphy.

Acknowledgments

This work was sponsored by Saudi Aramco. We thank the management of Saudi Aramco for permission to publish this work. We express our thankfulness and gratitude to Dr. Aus Al-Tawil (SARCD manager, Saudi Aramco) for his endless outstanding support and motivations during all phases of this study. We also thank Dr. Yves-Michel Le Nindre, Dr. Denis Vaslet, Prof. J. Fred Read, and Dr. Langhorne Smith for providing valuable suggestions and constructive comments. We also extend our thanks to Dr. Raed Al-Dukhayyil for field support. We thank Prof. Volker Vahrenkamp, Dr. Frans S.P. van Buchem and Dr. Christopher Toland who post-edited the English style and grammar.

Reference

Abu-Ali, M., Littke, R., 2005. Paleozoic petroleum systems of Saudi Arabia: a basin modeling approach. GeoArabia, 10(3), 131-168.

Adams, J.E., Rhodes, M.L., 1960. Dolomitization by seepage refluxion. American Association of Petroleum Geologists Bulletin, 44, 1912-1920.

Ahlbrandt, T.S., 2002. Madbi Amran/Qishn total petroleum system of the Ma'Rib-Al Jawf/Shabwah, and Masila-Jeza basins, Yemen (No. 2202-G).

Aigner, T., 1985, Storm depositional systems; dynamic stratigraphy in modern and ancient shallow-marine sequences: Storm depositional systems; dynamic stratigraphy in modern and ancient shallow-marine sequences: Berlin, Federal Republic of Germany (DEU), Springer-Verlag, Berlin, 174 pp.

Al-Awwad, S.F., Collins, L.B., 2013a. Arabian carbonate reservoirs: A depositional model of the Arab-D reservoir in Khurais field, Saudi Arabia. AAPG bulletin, 97(7), 1099-1119

Al-Awwad, S.F., Collins, L.B., 2013b. Carbonate-platform scale correlation of stacked high-frequency sequences in the Arab-D reservoir, Saudi Arabia. Sedimentary Geology, 294, 205-218.

Al-Awwad, S.F., Pomar, L., 2015. Origin of the rudstone-floatstone beds in the Upper Jurassic Arab-D reservoir, Khurais Complex, Saudi Arabia. Marine and Petroleum Geology, 67, 743-768.

Al-Husseini, M., Matthews, R.K., Mattner, J., 2006. Stratigraphic Note: Orbital-forcing calibration of the Late Jurassic (Oxfordian-early Kimmeridgian) Hanifa Formation, Saudi Arabia. GeoArabia 11, 145-149.

Al-Mojel, A., 2017. Sedimentology and sequence stratigraphy of the Jurassic, Jebal Tuwaiq, Central Saudi Arabia. Ph.D. Thesis, Univ. Bordeaux 3, Bordeaux, France.

Al-Mojel, A., Dera, G., Razin, P., Le Nindre, Y.M., 2018. Carbon and oxygen isotope stratigraphy of Jurassic platform carbonates from Saudi Arabia: Implications for diagenesis, correlations and global paleoenvironmental changes. Palaeogeography, Palaeoclimatology, Palaeoecology, 511, 388-402.

Al-Mojel, A., Kerans, C., 2014. The Sedimentology and Sequence Stratigraphy of the Hanifa Formation Outcrop, Wadi Birk, Saudi Arabia. 11th Middle East Geosciences Conference, GEO 2014. GeoArabia, Abstract, 10-12 March 2014, Manama, Bahrain.

Al-Naji, N.S. 2002. Two carbonate shelf margins with hydrocarbon potential compared: Upper Jurassic formations of Arabian Basin and Guadalupian formations of Permian Basin of Texas and New Mexico. M.S Thesis, University of South Carolina, 234 p.

Al-Suwaidi, A.S., Aziz, S.K., 2002. Sequence stratigraphy of Oxfordian and Kimmeridgian shelf carbonate reservoirs, offshore Abu Dhabi. GeoArabia, 7, 31-44.

Allenbach, R.P., 2001. Synsedimentary tectonics in an epicontinental sea: a new interpretation of the Oxfordian basins of northern Switzerland. Eclogae Geologicae Helvetiae, 94, 265-287.

Allenbach, R.P., 2002. The ups and downs of “Tectonic Quiescence”—recognizing differential subsidence in the epicontinental sea of the Oxfordian in the Swiss Jura Mountains. Sedimentary Geology, 150 (3), 323-342.

Alnazghah, M.H., Bádenas, B., Pomar, L., Aurell, M., Morsilli, M., 2013. Facies heterogeneity at interwell-scale in a carbonate ramp, Upper Jurassic, NE Spain. Marine and Petroleum Geology, 44, 140-163.

Ayres, M.G., Bilal, M., Jones, R.W., Slentz, L.W., Tartir, M., Wilson, A.O., 1982. Hydrocarbon habitat in main producing areas, Saudi Arabia. AAPG bulletin, 66(1), 1-9.

Bádenas, B., Pomar, L., Aurell, M., Morsilli, M., 2012. A facies model for internalites (internal wave deposits) on a gently sloping carbonate ramp (Upper Jurassic, Ricla, NE Spain). Sedimentary Geology, 271, 44-57.

Boesch, D.F., Rabalais, N.N., 1991. Effects of hypoxia on continental shelf benthos: comparisons between the New York Bight and the Northern Gulf of Mexico. Geological Society, London, Special Publications, 58(1), 27-34.

Bottjer, D. J., Arthur, M. A., Dean, W. E., Hattin, D. E., Savrda, C. E., 1986. Rhythmic bedding produced in Cretaceous pelagic carbonate environments: sensitive recorders of climatic cycles. Paleoceanography, 1(4), 467-481.

Brannan, J., Sahota G., Gerdes K.D., Berry J.A.L., 1999. Geological evolution of the central Marib-Shabwa basin, Yemen. GeoArabia, 4 (1), 9-34.

Bromley, R.G., Ekdale, A.A., 1984. Trace fossil preservation in flint in the European chalk. Journal of Paleontology, 58, 298-311.

Carruthers, A., Mckie, T., Price, J., Dyer, R., Williams, G., Watson, P., 1996. The application of sequence stratigraphy to the understanding of Late Jurassic turbidite plays in the Central North Sea, UKCS. Geological Society, London, Special Publications, 114(1), 29-45.

Chevalier, F., Garcia, J.P., Quesne, D., Guiraud, M., Menot, J.C., 2001. Correlations and genetic stratigraphy through Oxfordian reefal formations in the upper Yonne valley (southern Paris basin, France). Bulletin de la Société Géologique de France 172 (1), 69-84.

Colombié, C., Strasser, A., 2005. Facies, cycles, and controls on the evolution of a keep-up carbonate platform (Kimmeridgian, Swiss Jura). Sedimentology, 52(6), 1207-1227.

Dardeau, G., Atrops, F., Fortwengler, D., de Graciansky, P.C., Marchand, D., 1988. Jeu de blocs et tectonique distensive au Callovien et à l'Oxfordien dans le bassin du Sud-Est de la France. Bulletin de la Société géologique de France, 8(IV), 771-777.

Donnadieu, Y., Dromart, G., Goddéris, Y., Pucéat, E., Brigaud, B., Dera, G., Dumas, C. Olivier, N., 2011. A mechanism for brief glacial episodes in the Mesozoic greenhouse. Paleoceanography 26.

Dromart, G., Garcia, J.P., Picard, S., Atrops, F., Lécuyer, C., Sheppard, S.M.F., 2003a. Ice age at the Middle-Late Jurassic transition? Earth and Planetary Science Letters. 213, 205-220.

Dromart, G., Garcia, J.P., Picard, S., Rousseau, M., Atrops, F., Lécuyer, C., Sheppard, S.M.F., 2003b. Perturbation of the carbon cycle at the Middle/Late Jurassic transition: geological and geochemical evidence. American Journal of Science 303, 667-707.

Droste, H., 1990. Depositional cycles and source rock development in an epeiric intra-platform basin: the Hanifa Formation of the Arabian Peninsula. Sedimentary Geology, 69(3-4), 281-296.

Duke, W.L., 1985. Hummocky cross-stratification, tropical hurricanes, and intense winter storms. Sedimentology, 32(2), 167-194.

Dunham, R.J., 1962. Classification of carbonate rocks according to depositional texture. In: Ham, W.E. (Ed.), Classification of Carbonate Rocks: AAPG Memoir 1, 108-121. Tulsa, OK.

El-Asa'ad, G.M.A., 1992. Late Callovian Ammonites from the Tuwaiq Mountain Limestone of Saudi Arabia. Journal of King Saud University, 4(2), 173-184.

Embry, A.F., Klovan, J.E., 1971. A late Devonian reef tract on northeastern Banks Island, NWT. Bulletin of Canadian Petroleum Geology, 19(4), 730-781.

Enos, P., 1983. Shelf Environment: In: Scholle, P.A., Bebout, D.G., Moore, C.H. (Eds.), Carbonate Depositional Environments. American Association Petroleum Geologists Memoir, 33, 268-295.

Fallatah, M.I., Kerans, C., 2018. Stratigraphic evolution of the Late Jurassic Hanifa Formation along the Tuwaiq Escarpment, Saudi Arabia: Evidence for a carbonate ramp system. Sedimentary Geology, 363, 152-180.

Fischer, J.-C., Manivit, J., Vaslet, D., 2001. Jurassic gastropod faunas of central Saudi Arabia. GeoArabia (Manama), 6(1), 63-100.

Frébourg, G., Ruppel, S.C., Loucks, R.G., Lambert, J. 2016. Depositional controls on sediment body architecture in the Eagle Ford/Boquillas system: Insights from outcrops in west Texas, United States. AAPG Bulletin, 100(4), 657-682.

Galli, G., 1993. "Calcari Grigi" formation, Jurasic, Venetian Alps. In: Galli, G. (Ed.), Temporal and Spatial Patterns in Carbonate Platforms. Springer, Berlin, 97-129.

Goldring, R., Taylor, A.M., Hughes, G.W., 2005. The application of ichnofabrics towards bridging the dichotomy between siliciclastic and carbonate shelf facies: examples from the Upper Jurassic Fulmar Formation (U.K.) and the Jubaila Formation (Saudi Arabia). Proceedings of the Geologists' Association, 116(3-4), 235-249.

Gollesstaneh, A., 1965. A micropalaeontological study of the Upper Jurassic and Lower Cretaceous of Southern Iran (Doctoral dissertation, University of London).

Gradstein, F.M., Ogg, J.G., Schmitz, M.D., Ogg, G.M., 2012. The Geologic Time Scale 2012. Elsevier, p. 1144.

Hallam, A., 1988. A reevaluation of Jurassic eustasy in the light of new data and the revised Exxon curve.

Hallock, P., 2001. Coral reefs, carbonate sediments, nutrients, and global change. The history and sedimentology of ancient reef systems, 387-427.

Hallock, P., 2005. Global change and modern coral reefs: new opportunities to understand shallow-water carbonate depositional processes. Sedimentary Geology, 175(1), 19-33.

Hallock, P., Schlager, W., 1986. Nutrient excess and the demise of coral reefs and carbonate platforms. Palaios, 389-398.

Handford, C.R., Cantrell, D.L., Keith, T.H., 2002, Regional facies relationships and sequence stratigraphy of a super-giant reservoir (Arab-D Member), Saudi Arabia: Society of Economic Paleontologists Gulf Coast Section Research Conference Program and Abstracts 22, 539-563.

Haq, B.U., 2018. Jurassic sea-level variations: a reappraisal. GSA Today, 28(1).

Haq, B.U., Al-Qahtani, A.M., 2005. Phanerozoic cycles of sea-level change on the Arabian Platform. GeoArabia, 10(2), 127-160.

Hardenbol, J., Jacquin, T., Farley, M.B., de Graciansky, P.C., Vail, P.R., 1998. Mesozoic and Cenozoic sequence chronostratigraphic framework of European basins. In: de Graciansky, P. C., Hardenbol, J., Jaquin, T., Vail, P.R. (Eds.), Mesozoic and Cenozoic Sequence Stratigraphy of European Basins. Society for Sedimentary Geology (SEPM), Tulsa, 3-13.

Howarth, M.K., 1992. Tithonian and Berriasian ammonites from the Chia Gara Formation in northern Iraq. Palaeontology, 35(3), 597-655.

Hughes, G.W., 2009. Biofacies and palaeoenvironments of the Jurassic Shaqra Group of Saudi Arabia. Volumina Jurassica, v. 6, p. 33-45.

Hughes, G.W., Varol, O., Al-Khaled. M., 2008. Late Oxfordian micropalaentology, nanopalaentology and palaeoenvironments of Saudi Arabia. GeoArabia, 13 (2), 15-46.

Jacquemyn, C., Jackson, M., Hampson, G., John, C., Cantrell, D., Zühlke, R., AbuBshait, A., Lindsay, R., Monsen, R., 2017. Geometry, spatial arrangement and origin of carbonate grain-dominated, scour-fill and event-bed deposits: Late Jurassic Jubaila Formation and Arab-D Member, Saudi Arabia. Sedimentology. (Accepted Article).

Janson, X., Kerans, C., Loucks, R., Marhx, M.A., Reyes, C. and Murguia, F., 2011. Seismic architecture of a Lower Cretaceous platform-to-slope system, Santa Agueda and Poza Rica fields, Mexico. AAPG Bulletin, 95, 105-146.

Kadar, A.P., De Keyser, T., Neog, N., Karam, K.A., Le Nindre, Y.M., Davies, R.B., 2015. Calcareous nanofossil zonation and sequence stratigraphy of the Jurassic System, onshore Kuwait. GeoArabia, 20(4), 125-180.

Keho, T.H., Broadhead, M.K., Neves, F.A., 2009. Using an isochron to constrain amplitude analysis: A case study of a carbonate stratigraphic trap in Saudi Arabia. The Leading Edge, 28(11), 1304-1313.

Keupp, H., Jenisch, A., Herrmann, R., Neuweiler, F., Reitner, J., 1993. Microbial carbonate crusts-a key to the environmental analysis of fossil spongiolites? Facies, 29(1), 41-54.

Khetani, A.B., Read, J.F., 2002. Sequence development of a mixed carbonate-siliciclastic high-relief ramp, Mississippian, Kentucky, USA. Journal of Sedimentary Research, 72(5), 657-672.

Langdon, G.S., Malecek, S.J. 1987. Seismic stratigraphic study of two Oxfordian carbonate sequences, eastern Saudi Arabia. American Association of Petroleum Geologists Bulletin, 71 (4), 403-418.

Lannace, A., Frisia, S., 1994. Changing dolomitization styles from Norian to Rhaetian in the southern Tethys realm. In: Purser, B., Tucker, M., Zenger, D. (Eds.), Dolomites, A Volume in Honour of Dolomieu, International Association of Sedimentologists, Special Publication, 21, 75-89.

Le Nindre, Y.M., Manivit, J., Vaslet, D., 1990. Stratigraphie séquentielle du Jurassique et du Crétacé en Arabie Saoudite. Bulletin, Société géologique de France, Paris, sér. 8, VI, 1025-1034.

Leinfelder, R., 1993. Upper Jurassic reef types and controlling factors. A preliminary report. Profil 5, 1-45.

Leinfelder, R., 1994. Distribution of Jurassic reef types: a mirror of structural and environmental changes during breakup of Pangea. In: Embry, A.F., Beauchamp, B., Glass, D.J. (Eds.), Pangea: Global Environments and Resources. Canadian Society of Petroleum Geologists, Calgary, Memoir, 17, 677-700.

Lhamyani, B., 1985. Etude stratigraphique de l'Oxfordien dans l'arc de Castellane(Alpes-de-Haute-Provence): passage des faciès provençaux aux faciès dauphinois (Doctoral dissertation).

Lindsay, R.F., Cantrell, D.L., Hughes, G.W, Keith, T.H., Mueller III, H.W., Russell, D., 2006. Ghawar Arab-D reservoir: Widespread porosity in shoaling-upward carbonate cycles, Saudi Arabia: AAPG Memoir 88, 97-138.

Lukasik, J.J., James, N.P., McGowran, B., Bone, Y., 2000. An epeiric ramp: low-energy, cool-water carbonate facies in a Tertiary inland sea, Murray Basin, South Australia. Sedimentology, 47(4), 851-881.

Mancini, E.A., Obid, J.A., Puckett, T.M., 2004. Upper Jurassic transgressive-regressive sequences, Mississippi interior salt basin area.

Manivit J, Le Nindre, Y.M., Vaslet D., 1990. Le Jurassique d'Arabie Centrale. In Histoire Gologique de la Bordure Occidentale de la Plate-forme Arabe. Volume 4. Document du BRGM n°194.

Manivit, J., Pellaton, C., Vaslet, D., Le Nindre, Y.M., Brosse, J.M., Fourniguet, J., 1985a. Geologic map of the Wadi al Mulayh quadrangle, sheet 22H, Kingdom of Saudi Arabia. Saudi Arabian Deputy Ministry for Mineral Resources Geosciences Map, GM-92, scale, 1(250,000), 1-32.

Manivit, J., Pellaton, C., Vaslet, D., Le Nindre, Y.M., Brosse, J.M., Breton, J.P., Fourniguet, J., 1985b. Geologic map of the Darma quadrangle, sheet 24H, Kingdom of Saudi Arabia. Saudi Arabian Deputy Ministry for Mineral Resources Geosciences Map, GM-101, scale, 1(250,000), 133.

Mattner, J., Al-Husseini, M., 2002. Essay: Applied cyclo-stratigraphy for the Middle East E&P industry. GeoArabia, 7 (4), 734-744.

McGuire, M.D., 2003. Sequence Stratigraphy of the Hanifa Reservoir in Berri Field, Saudi Arabia. In American Association of Petroleum Geologists Conference, Salt Lake City, Abstract (No. 78653).

McGuire, M.D., Koepnick, R.B., Markello, M.L., Stockton, M.L., Waite, L.E., Kompanik, M.J., Al-Shammary, M.J., AlAmoudi, M.O., 1993. Importance of sequence stratigraphic concepts in development of reservoir architecture in Upper Jurassic grainstones, Hadriya and Hanifa reservoirs, Saudi Arabia. Society of Petroleum Engineers, 489-499.

McKenzie, J.A., Hsu, K.J., Schneider, J.F., 1980. Movement of subsurface waters under the sabkha, Abu Dhabi, UAE, and its relation to evaporative dolomite genesis, in Zenger, D.H., et al., eds., Concepts and models of dolomitization: Society of Economic Paleontologists and Mineralogists Special Publication, 28, 11-30.

Meyer, F.O., Price, R.C., 1993. A new Arab-D depositional model, Ghawar Field, Saudi Arabia. In: Paper Presented at the Middle East Oil Show, Bahrain.

Meyer, F.O., Price, R.C., Al-Ghamdi, I.A., Al-Goba, I.M., Al-Raimi, S.M., Cole, J.C., 1996. Sequential stratigraphy of outcropping strata equivalent to Arab-D Reservoir, Wadi Nisah, Saudi Arabia. GeoArabia (Manama) 1 (3), 435-456.

Mitchell, J.C., Lehmann, P.J., Cantrell, D.L., Al-Jallal, I.A., Al-Thagafy, M.A.R., 1988. Lithofacies, diagenesis and depositional sequence: Arab-D Member, Ghawar Field, Saudi Arabia. SEPM Core Workshop 12, 459-514.

Morsilli, M., Pomar, L., 2012. Internal waves vs. surface storm waves: a review on the origin of hummocky cross-stratification. Terra Nova, 24(4), 273-282.

Mullins, H.T., Cook, H.E., 1986. Carbonate apron models: alternatives to the submarine fan model for paleoenvironmental analysis and hydrocarbon exploration. Sedimentary Geology, 48, 37-79.

Murris, R.J., 1980. Middle East: Stratigraphic evolution and oil habitat. AAPG Bulletin, 64,597–618.

Myrow, P.M., Southard, J.B., 1996. Tempestite deposition. Journal of Sedimentary Research, 66 (5).

Nunn, E.V., Price, G.D., 2010. Late Jurassic (Kimmeridgian–Tithonian) stable isotopes (δ 18 O, δ 13 C) and Mg/Ca ratios: new palaeoclimate data from Helmsdale, northeast Scotland. Palaeogeography, Palaeoclimatology, Palaeoecology, 292(1), 325-335.

Nunn, E.V., Price, G.D., Hart, M., Page, K., Leng, M., 2009. Isotopic signals from CallovianeKimmeridgian (Middle Upper Jurassic) belemnites and bulk organic carbon, Staffin Bay, Isle of Skye, Scotland. Journal of the Geological Society, London 166, 633e641.

Pellenard, P., Tramoy, R., Pucéat, E., Huret, E., Martinez, M., Bruneau, L., Thierry, J., 2014. Carbon cycle and sea-water palaeotemperature evolution at the Middle-Late Jurassic transition, eastern Paris Basin (France). Marine and Petroleum Geology, 53, 30-43.

Pittet, B., Strasser, A., 1998. Long-distance correlations by sequence stratigraphy and cyclostratigraphy: examples and implications (Oxfordian from the Swiss Jura, Spain, and Normandy). Geol. Rundschau, 86 (4), 852-874.

Pomar, L., Hallock, P., 2008. Carbonate factories: a conundrum in sedimentary geology. Earth-Science Reviews, 87(3), 134-169.

Powers, R.W., 1962. Arabian Upper Jurassic carbonate reservoir rocks. In: Ham W.E. (Ed.), Classification of Carbonate Rocks: A Symposium. American Association of Petroleum Geologists, Memoir 1, 122-192.

Powers, R.W., 1968. Lexique Stratigraphique International, v.III, Asie, 10bl, Saudi Arabia. Centre National de la Recherche Scientifique, Paris, 177p.

Powers, R.W., Ramirez, L.F., Redmond, C.D., Elberg, E.L., 1966. Geology of the Arabian Peninsula, Geological Survey Professional Paper, 560-D, 147p.

Rabalais, N.N., Turner, R.E., Wiseman Jr,W.J., 2002. Gulf of Mexico hypoxia, aka “The dead zone”. Annual Review of ecology and Systematics, 33(1), 235-263.

Rabalais, N.N., Turner, R.E., Wiseman, W.J., Boesch, D.F., 1991. A brief summary of hypoxia on the northern Gulf of Mexico continental shelf: 1985–1988. Geological Society, London, Special Publications, 58(1), 35-47.

Razin, P., Grélaud, C., van Buchem, F., 2017. The mid-Cretaceous Natih Formation in Oman: A model for carbonate platforms and organic-rich intrashelf basins. AAPG Bulletin, 101(4), 515-522.

Razin, P., Taati, F., Van Buchem, F.S.P., 2010. Sequence stratigraphy of Cenomanian–Turonian carbonate platform margins (Sarvak Formation) in the High Zagros, SW Iran: an outcrop reference model for the Arabian Plate. Geological Society, London, Special Publications, 329(1), 187-218.

Reinson, G.E., 1979. Facies models 14. Barrier island systems. Geoscience Canada, 6(2). 51-68

Reynolds, A.D., 1995. Sedimentology and sequence stratigraphy of the Thistle field, northern North Sea. Norwegian Petroleum Society Special Publications, 5, 257-271.

Riding, R., 2000. Microbial carbonates: the geological record of calcified bacterial-algal mats and biofilms. Sedimentology, 47 (Supplement 1), p. 179-214.

Riding, R., Liang, L., 2005. Geobiology of microbial carbonates: metazon and seawater saturation state influences on secular trends during the Phanerozoic. Palaeogeography, Palaeoclimatology, Palaeoecology, 219, 101-85.

Rousseau, M., Dromart, G., Droste, H., Homewood, P., 2006. Stratigraphic organisation of the Jurassic sequence in Interior Oman, Arabian Peninsula. GeoArabia,11(1), 17.

Sadooni, F.N., 1997. Stratigraphy and petroleum prospects of Upper Jurassic carbonates in Iraq. Petroleum Geoscience, 3, (3),233-243.

Schieber, J., Southard, J., Thaisen, K., 2007. Accretion of mudstone beds from migrating floccule ripples. Science, 318(5857), 1760-1763.

Schieber, J., Southard, J.B., Kissling, P., Rossman, B., Ginsburg, R., 2013. Experimental deposition of carbonate mud from moving suspensions: importance of flocculation and implications for modern and ancient carbonate mud deposition. Journal of Sedimentary Research, 83(11), 1025-1031.

Scotese, C.R., 2003. Paleomap project, Earth History and Climate History, Late Jurassic. Paleomap, URL http://www.Scotese.com/late1.htm

Sharief, F.A., Khan M.S., Magara, K., 1991. Outcrop-Subcrop Sequence and Diagenesis of Upper Jurassic Arab-Hith Formations, Central Saudi Arabia. Journal KAU, Earth Science, 4, 105-136.

Sharland, P.R., Archer R., Casey D.M., Davies R.B., Hall S.H., Heward A.P., Horbury A.D., Simmons M.D., 2001. Arabian Plate Sequence Stratigraphy. GeoArabia Special Publication 2, Gulf PetroLink, Bahrain, 371.

Steineke, M.R.A., Bramkamp, R.A., Sander, N.J., 1958. Stratigraphic relations of Arabian Jurassic oil. In: Weeks, L.G. (Ed.), Habitat of Oil. American Association of Petroleum Geologists Symposium, 1294-1329.

Strasser, A., Hillgärtner, H., Hug, W., Pittet, B., 2000. Third-order depositional sequences reflecting Milankovitch cyclicity. Terra Nova, 12(6), 303-311.

Strasser, A., Pittet, B., Hug, W., 2015. Palaeogeography of a shallow carbonate platform: The case of the Middle to Late Oxfordian in the Swiss Jura Mountains. Journal of Palaeogeography, 4 (3), 251-268.

Strasser, A., Védrine, S., 2009. Controls on facies mosaics of carbonate platforms: a case study from the Oxfordian of the Swiss Jura. In: Swart, P.K., Eberli, G.P., McKenzie, J.A. (Eds.), Perspectives in Sedimentary Geology: A Tribute to the Career of Robert Nathan Ginsburg. International Association of Sedimentologists. Special Publication, 41. Blackwell, Oxford, 41, 199-213.

Swart, P.K., Cantrell, D.L., Westphal, H., Handford, C.R., Kendall, C.G., 2005. Origin of dolomite in the Arab-D reservoir from the Ghawar Field, Saudi Arabia: evidence from petrographic and geochemical constraints. Journal of Sedimentary Research, 75(3), 476-491.

Thierry, J., Barrier, E., Vaslet, D., Le Metour, J., Le Nindre.Y.M., and Ziegler, M., 2000. Early Tithonian (141-139 Ma), Paris: Dercourt, J., Gaetani, M. et al. (Eds.), Atlas Peri-Tethys, Palaegeographical maps, CCGM/CGMW, Carte/map 11.

Turner, R.E., Rabalais, N.N., 1994. Coastal eutrophication near the Mississippi river delta. Nature, 368(6472), 619.

Vaslet, D., Brush, J.M., Breton, J.P., Manivit, J., Le Strat, P., Fourniguet, J., Shorbaji, H., 1988. Geologic map of the quadrangle Shaqra, sheet 25H. Kingdom of Saudi Arabia: Deputy Ministry for Mineral Resources Geoscience Map GM-120C, 29.

Vaslet, D., Delfour, J., Manivit, J., Le Nindre, Y.M., Brosse, J.M., Fourniquet, J., 1983. Geologic map of the Wadi ar Rayn Quadrangle, sheet 23H, Kingdom of Saudi Arabia (with text). Saudi Arabian Deputy Ministry for Mineral Resources, Jeddah, Geosciences Map GM-63A, 1-46.

Vaslet, D., Pellaton, C., Manivit, J., Le Nindre, Y.M., Brosse, J.M., Fourniguet, J., 1985. Geologic map of the Sulayyimah quadrangle, sheet 21 H, Kingdom of Saudi Arabia. Scale 1:250.000. Geoscience Map GM 100 A. Jeddah, Saudi Arabia A.H. 1405. Ministry of Petroleum and Mineral Resources.

Védrine, S., Strasser, A., 2009. High-frequency palaeoenvironmental changes on a shallow carbonate platform during a marine transgression (Late Oxfordian, Swiss Jura Mountains). Swiss journal of geosciences, 102(2), 247-270.

Walley, C.D., 1985. Depositional history of southern Tunisia and northwestern Libya in Mid and Late Jurassic time. Geological Magazine, 122(03), 233-247.
Wilson, J.L., 1975. Carbonate Facies in Geologic History. Springer-Verlag, New York, 471 pp.
Wilson, J.L., Jordan, C., 1983. Middle Shelf Environment. In: Scholle, P.A., Bebout, D.G., Moore, C.H. (Eds.), Carbonate Depositional Environments. American Association Petroleum Geologists Memoir, 33, 345-440.
Ziegler, M.A., 2001. Late Permian to Holocene Paleofacies evolution of the Arabian plate and its hydrocarbon occurrences. GeoArabia, 6, 445-504.

Figure captions

Figure 1: Geological map of the study area showing the Jurassic outcrops and measured sections, modified from Fischer et al. (2001). The measured sections are: (1) Huraymila/Wadi Malham, (2) Khashm Qaddiyah, (3) Wadi Al-Ain, (4) Wadi Al Hawtah/Al Hawtah city, (5) Wadi Birk, (6) Wadi Gulghul, (7) As Sitarah, (8) Wadi Al-Haddar. The faults are mapped in the 1:250,00-scale quadrangles of Wadi al Mulayh (Manivit et al., 1985a), Wadi Ar Rayn (Vaslet et al., 1983), Darma (Manivit et al., 1985b) and Shaqra (Vaslet et al., 1988).

Figure 2: Paleogeographic map of the Late Jurassic showing the study area located in the southern margin of the Neo-Tethys Ocean corresponding to an extensive wide shallow-marine continental shelf close to western hinterland. (Scotese, 2003).

Figure 3: Lithostratigraphy and sequence stratigraphy of the Late Jurassic in Jabal Tuwaiq.The biostratigraphical scheme is from Manivit et al. (1990) and Fischer et al. (2001). The Middle Jurassic Late Callovian age is dated out of the study area (Mu'ayshibah 25° 34’ N) in argillaceous limestone facies at the base of T3 unit of the Tuwaiq Mountain Limestone (El-Asa’ad, 1992). See Fig. 4 and Fig. 15 for detailed legends.

Figure 4: High-resolution sequence stratigraphic cross-section of the Hanifa Formation.

Figure 5: High-resolution sequence stratigraphic cross-section of the Jubaila Limestone and Arab-D Member. For symbol legend see Fig. 4 and 15.

Figure 6: Arid evaporitic shoreline and lagoon facies association, A) F1 Anhydrite solution collapse breccia overlain by highly deformed and rotated units, B) F1 Collapse breccia including cm- to dm-sized clasts of limestone and dolomite, between Arab-D and Arab-C Mb, C) F2 Grayish red dolomite

with silicified evaporite nodules (red arrows), D) F2 Mud-supported very-fine to fine rhombic dolomite crystals with weakly fabric preserving texture.

Figure 7: Mixed carbonate-siliciclastic inner-lagoon facies association. A) F3 Large-scale cross-bedded and wave-ripple laminated (arrow) sandstone, B) F4 Calcareous shale, C) F4 Argillaceous mudstone/wackestone rich with sponge spicules,, D) F5 Slightly argillaceous nodular horizontal bioturbated peloidal wackestone/lime-mudstone, E) Photomicrographs of F5 with benthic foraminifera (*Kurnubia jurassica*; k arrows) and sponge spicules (s arrows),

Figure 8: Carbonate inner-platform facies association. A) F6 Thinly laminated lime-mudstone with hummocky-cross stratification, B) Photomicrographs of F6 shows thin lamination (red dash lines) with silt quartz grains (yellow arrows), C) F7 Bioturbated peloidal lime-mudstone to packstone overlain by F6 non-bioturbated thinly laminated lime-mudstone, C) Photomicrographs of F7 with benthic foraminifera (*Kurnubia jurassica*, k arrow; *Alveosepta Jaccardi*, a arrow) and quartz grains (q arrows), E) F8 Sharp-based Intraclast peloidal skeletal grainstone shows hummocky-, swaley- and plane-laminated sedimentary structures, F) Photomicrographs of F8 with dasyclad (*Clypeina*; d arrow), G) Interbedding of cross-bedded grainstone (F7) and thinly laminated lime-mudstone (F6) with soft-sediment deformation (Note: oblique view).

Figure 9: Barrier to back-barrier lagoon facies association. A) F9 Oncoidal grainstone and rudstone, B) Photomicrographs of F9 shows type 3 oncoid with sub-elliptical shapes and wavy lamination (yellow arrow), C) F10 Coral/stromatoporoid buildup, lime-mudstone/wackestone and floatstone, Hanifa Formation (Note: hammer for scale), D) F10 Biostromal rudist packstone to grainstone and floatstone, Jubaila Limestone, Wadi Malham (The first record of the Jurassic rudists in Saudi Arabia *Plesiodiceras* sp. identified by S. Schneider, personal communication), E) F11 Slightly bioturbated, swaley cross stratification (SCS) and trough cross-bedded medium peloidal grainstone (shoal), Hanifa Formation, F) Photomicrographs of F11 shows well-sorted cross-bedded (red dash lines) peloidal coated-grain grainstone, G) F11 Well-sorted very-fine to fine peloidal grainstone shows hummocky cross-stratification (HCS) (back-barrier washover), Hanifa Formation

Figure 10: Outcrop photo shows the relationship between the erosional-based storm-generated grainstones (F8) and the shallow-marine facies coral/stromatoporoid boundstone (10), Jubaila Limestone, Wadi Malham (HFS1 of JCS2).

Figure 11: Ideal depositional sequence models of the Hanifa composite sequences from West (proximal) to East (distal) showing spatial facies distributions and platform evolution in series of times (T0 to T5). Derived from the outcrop oblique-strike section in Figure 4.

Figure 12: Ideal depositional sequence models of the Jubaila-Arab-D composite sequences from west (proximal) to east (distal) showing spatial facies distributions and platform evolution in series of times (T0 to T9). Derived from the outcrop oblique-strike section in Figure 5.

Figure 13: A) West-east sequence stratigraphic correlation from surface to subsurface using gamma-ray logs. Khashm Ad Dhibi and Khashm Al-Qaddiyah is a composite gamma-ray logs of shallow cores penetrating the Middle and Late Jurassic. B) Paleofacies maps of Ziegler (2001).

Figure 14: Surface-to-subsurface high-resolution sequence stratigraphic correlation of the Jubaila-Arab-D sequence.

Figure 15: Depositional sequence model and long-term facies evolution of the Jubaila-Arab-D sequence of the Arabian Basin.

Figure 16: Late Jurassic geological history shows a comparison between the central Arabia sequences (defined herein) and the European standard sequences.

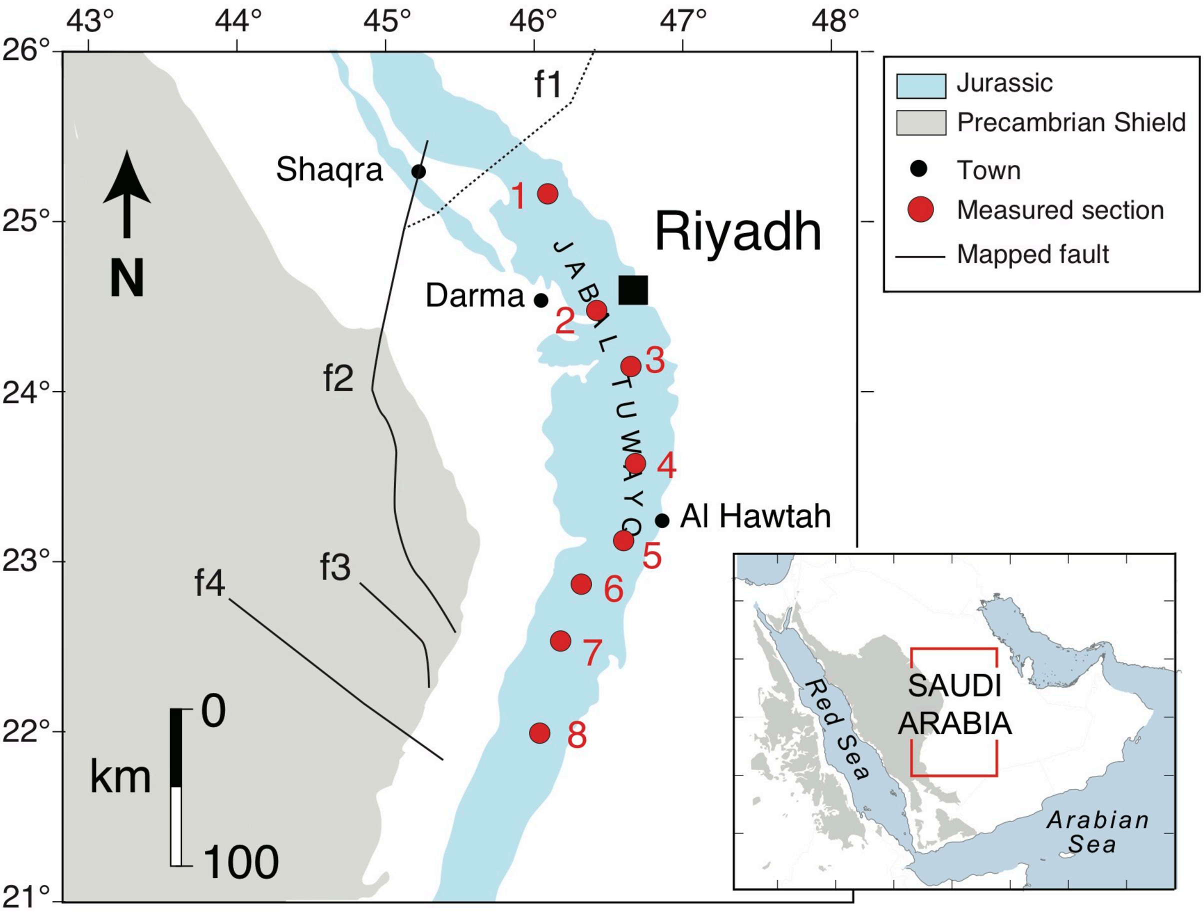

43°
44°
45°
46°
47°
48°
26°
25°
24°
23°
22°
21°
N
Shaqra
f1
1
Riyadh
JABAL TUWAYQ
Darma
2
3
f2
4
Al Hawtah
5
6
f3
f4
7
8
0
km
100
Jurassic
Precambrian Shield
Town
Measured section
Mapped fault
Red Sea
SAUDI ARABIA
Arabian Sea

Figure 1

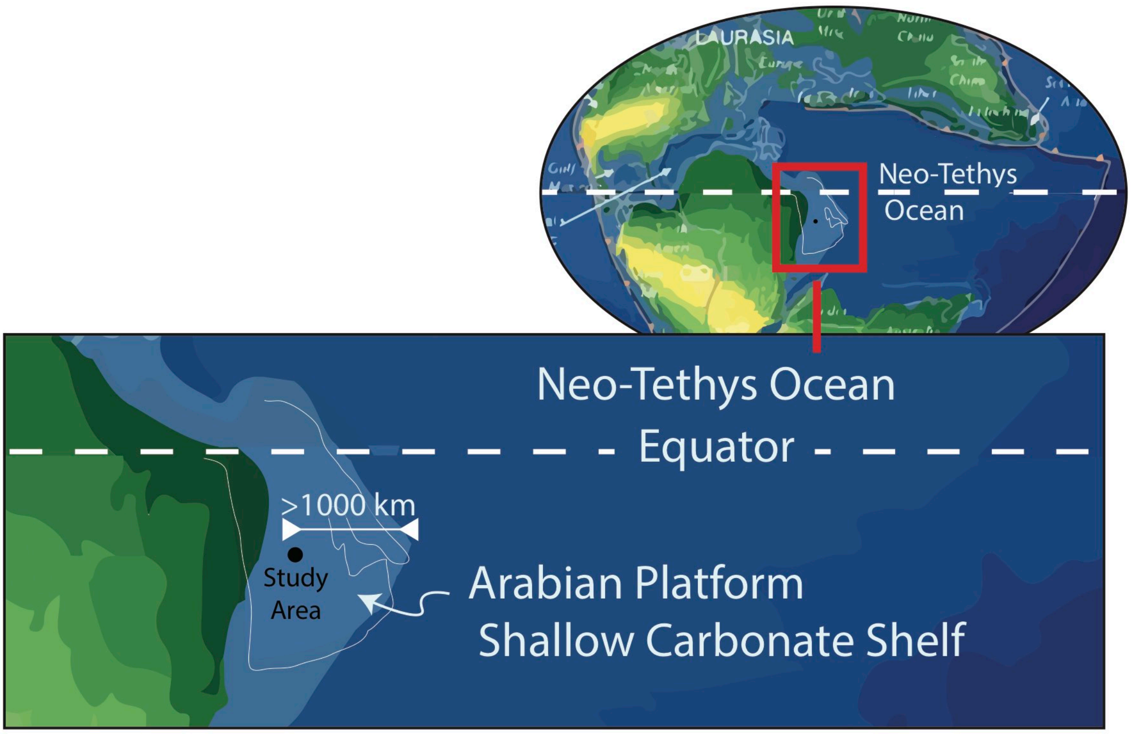
LAURASIA
Neo-Tethys
Ocean
Neo-Tethys Ocean
Equator
>1000 km
Study
Area
Arabian Platform
Shallow Carbonate Shelf

Figure 2.

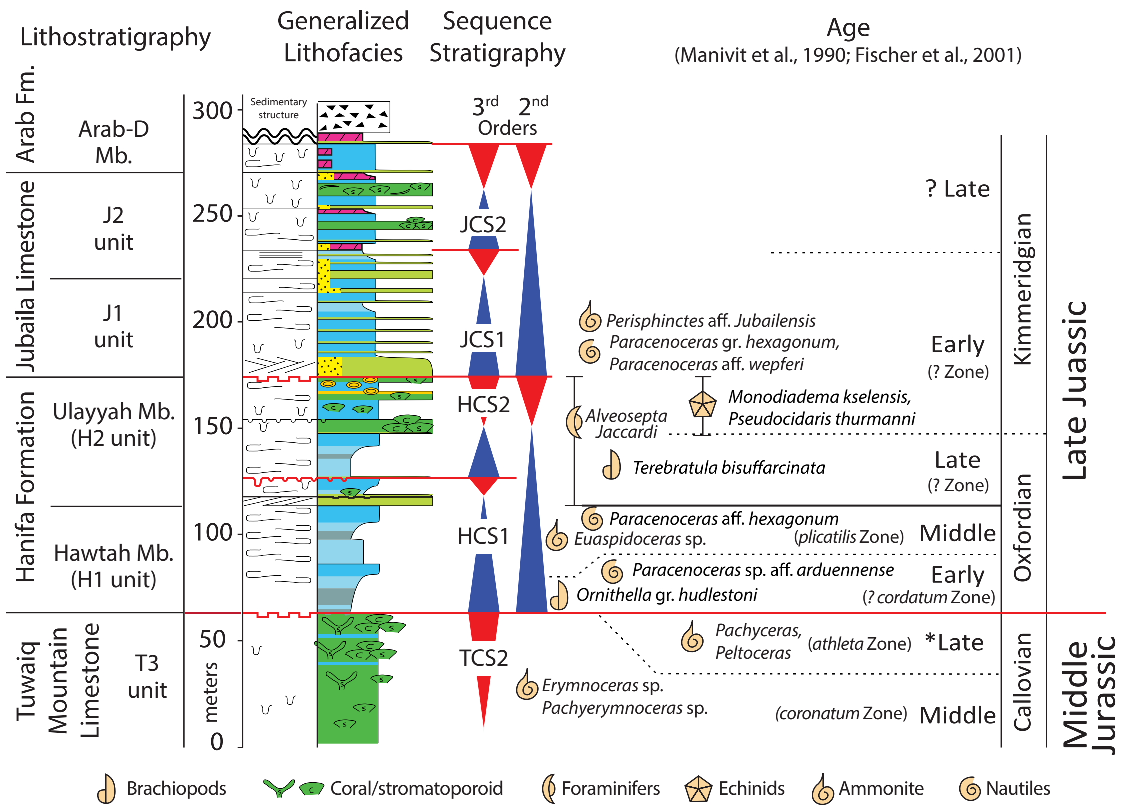

Lithostratigraphy
Generalized Lithofacies
Sequence Stratigraphy
Age
(Manivit et al., 1990; Fischer et al., 2001)
Arab Fm.
Arab-D Mb.
Jubaila Limestone
J2 unit
J1 unit
Hanifa Formation
Ulayyah Mb. (H2 unit)
Hawtah Mb. (H1 unit)
Tuwaiq Mountain Limestone
T3 unit
300
250
200
150
100
50
0
meters
Sedimentary structure
3rd 2nd Orders
JCS2
JCS1
HCS2
HCS1
TCS2
? Late
Perisphinctes aff. Jubailensis
Paracenoceras gr. hexagonum,
Paracenoceras aff. wepferi
Early
(? Zone)
Kimmeridgian
Alveosepta Jaccardi
Monodiadema kselensis,
Pseudocidaris thurmanni
Terebratula bisuffarcinata
Late
(? Zone)
Late Juassic
Paracenoceras aff. hexagonum
Euaspidoceras sp.
(plicatilis Zone)
Middle
Paracenoceras sp. aff. arduennense
Early
Ornithella gr. hudlestoni
(? cordatum Zone)
Oxfordian
Pachyceras,
Peltoceras
(athleta Zone)
*Late
Erymnoceras sp.
Pachyerymnoceras sp.
(coronatum Zone)
Middle
Callovian
Middle Jurassic
Brachiopods
Coral/stromatoporoid
Foraminifers
Echinids
Ammonite
Nautiles

Figure: 3

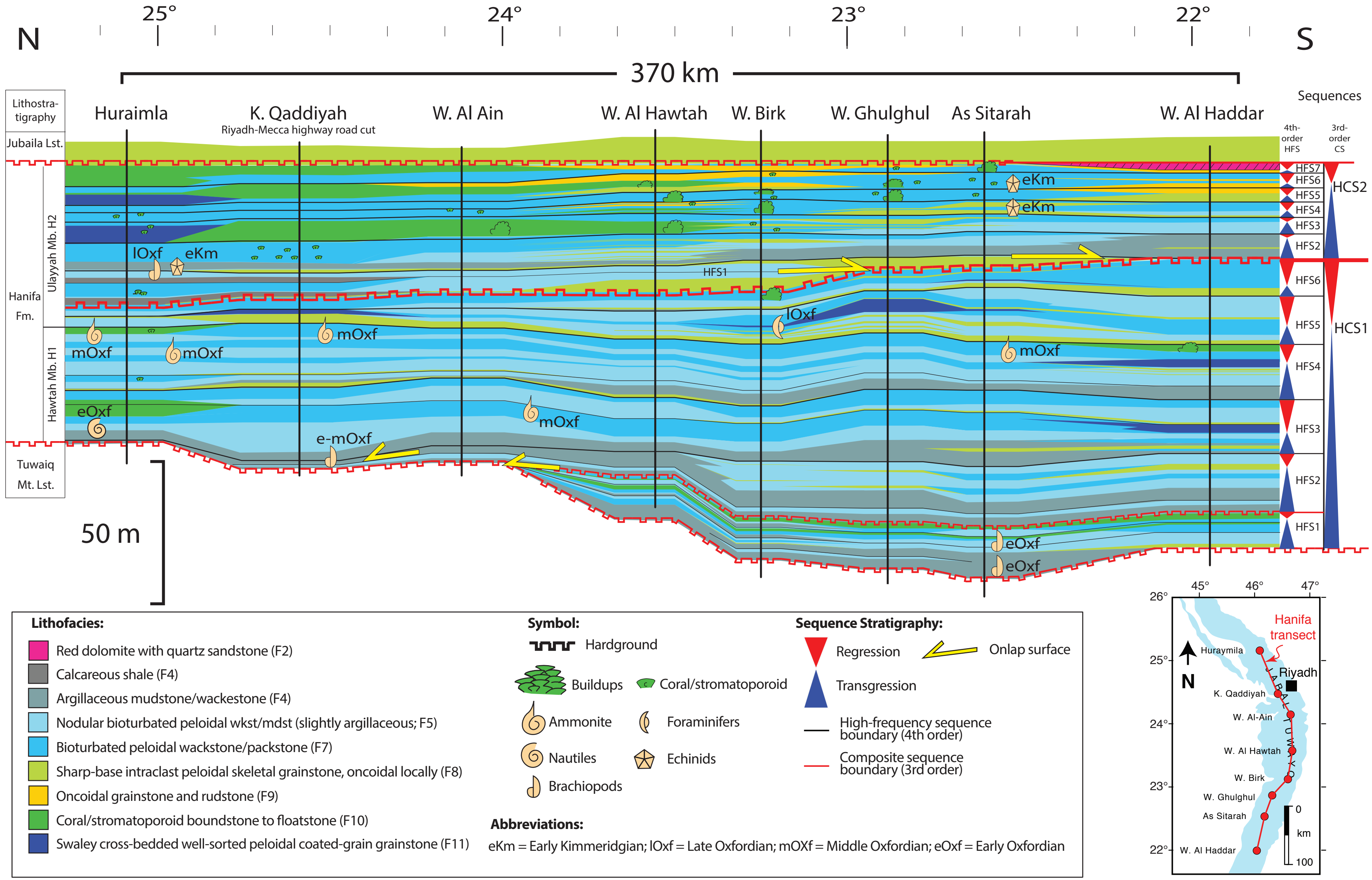

N
S
25°
24°
23°
22°
370 km
Lithostra-tigraphy
Jubaila Lst.
Hanifa Fm.
Ulayyah Mb. H2
Hawtah Mb. H1
Tuwaiq Mt. Lst.
Huraimla
K. Qaddiyah
Riyadh-Mecca highway road cut
W. Al Ain
W. Al Hawtah
W. Birk
W. Ghulghul
As Sitarah
W. Al Haddar
Sequences
4th-order HFS
3rd-order CS
HFS7
HFS6
HFS5
HFS4
HFS3
HFS2
HFS1
HCS2
HCS1
lOxf
eKm
mOxf
eOxf
e-mOxf
50 m
Lithofacies:
Red dolomite with quartz sandstone (F2)
Calcareous shale (F4)
Argillaceous mudstone/wackestone (F4)
Nodular bioturbated peloidal wkst/mdst (slightly argillaceous; F5)
Bioturbated peloidal wackstone/packstone (F7)
Sharp-base intraclast peloidal skeletal grainstone, oncoidal locally (F8)
Oncoidal grainstone and rudstone (F9)
Coral/stromatoporoid boundstone to floatstone (F10)
Swaley cross-bedded well-sorted peloidal coated-grain grainstone (F11)
Symbol:
Hardground
Buildups
Coral/stromatoporoid
Ammonite
Foraminifers
Nautiles
Echinids
Brachiopods
Sequence Stratigraphy:
Regression
Onlap surface
Transgression
High-frequency sequence boundary (4th order)
Composite sequence boundary (3rd order)
Abbreviations:
eKm = Early Kimmeridgian; lOxf = Late Oxfordian; mOXf = Middle Oxfordian; eOxf = Early Oxfordian
26°
25°
24°
23°
22°
45°
46°
47°
Hanifa transect
N
Huraymila
Riyadh
K. Qaddiyah
W. Al-Ain
W. Al Hawtah
W. Birk
W. Ghulghul
As Sitarah
W. Al Haddar
0
km
100

Figure 4

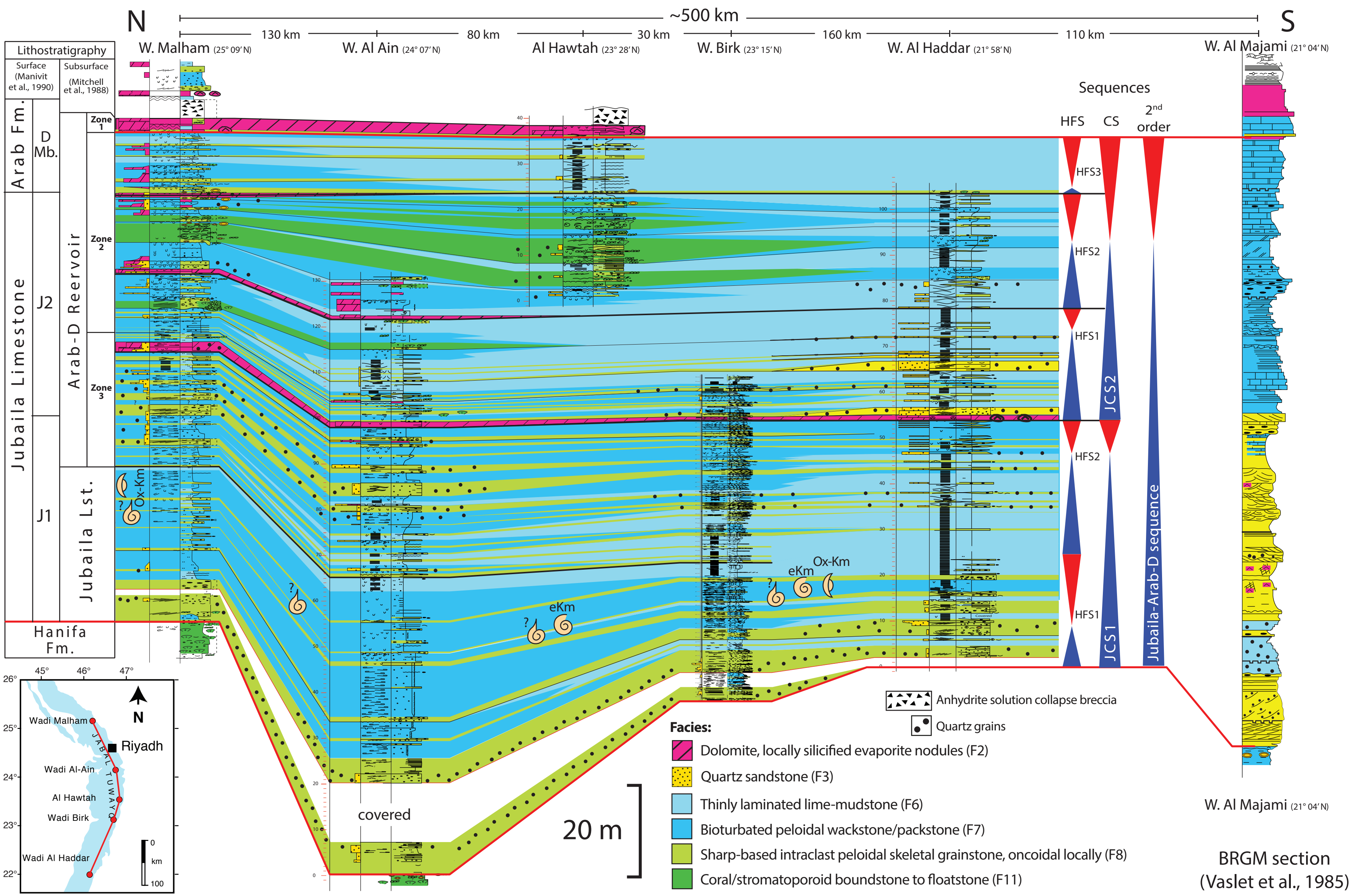

N
S
~500 km
130 km
80 km
30 km
160 km
110 km
W. Malham (25° 09' N)
W. Al Ain (24° 07' N)
Al Hawtah (23° 28' N)
W. Birk (23° 15' N)
W. Al Haddar (21° 58' N)
W. Al Majami (21° 04' N)
Lithostratigraphy
Surface (Manivit et al., 1990)
Subsurface (Mitchell et al., 1988)
Arab Fm.
D Mb.
Jubaila Limestone
J2
J1
Arab-D Reervoir
Zone 1
Zone 2
Zone 3
Jubaila Lst.
Hanifa Fm.
Ox-Km
eKm
covered
20 m
Sequences
HFS
CS
2nd order
HFS3
HFS2
HFS1
JCS2
JCS1
Jubaila-Arab-D sequence
Anhydrite solution collapse breccia
Quartz grains
Facies:
Dolomite, locally silicified evaporite nodules (F2)
Quartz sandstone (F3)
Thinly laminated lime-mudstone (F6)
Bioturbated peloidal wackstone/packstone (F7)
Sharp-based intraclast peloidal skeletal grainstone, oncoidal locally (F8)
Coral/stromatoporoid boundstone to floatstone (F11)
BRGM section (Vaslet et al., 1985)
Wadi Malham
Riyadh
Wadi Al-Ain
Al Hawtah
Wadi Birk
Wadi Al Haddar
JABAL TUWAYQ
45°
46°
47°
26°
25°
24°
23°
22°
km
0
100

Figure 5

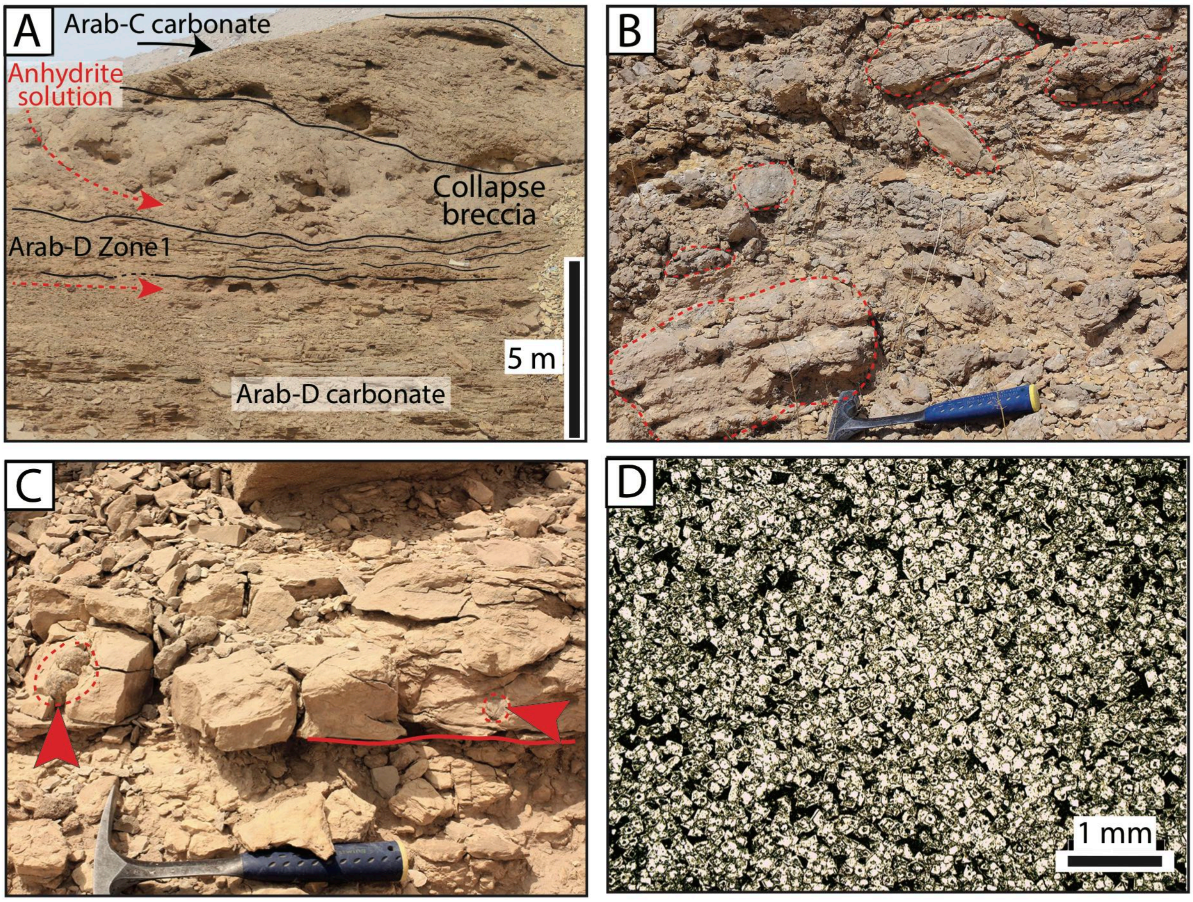
A
Arab-C carbonate
Anhydrite solution
Collapse breccia
Arab-D Zone1
5 m
Arab-D carbonate
B
C
D
1 mm

Figure 6

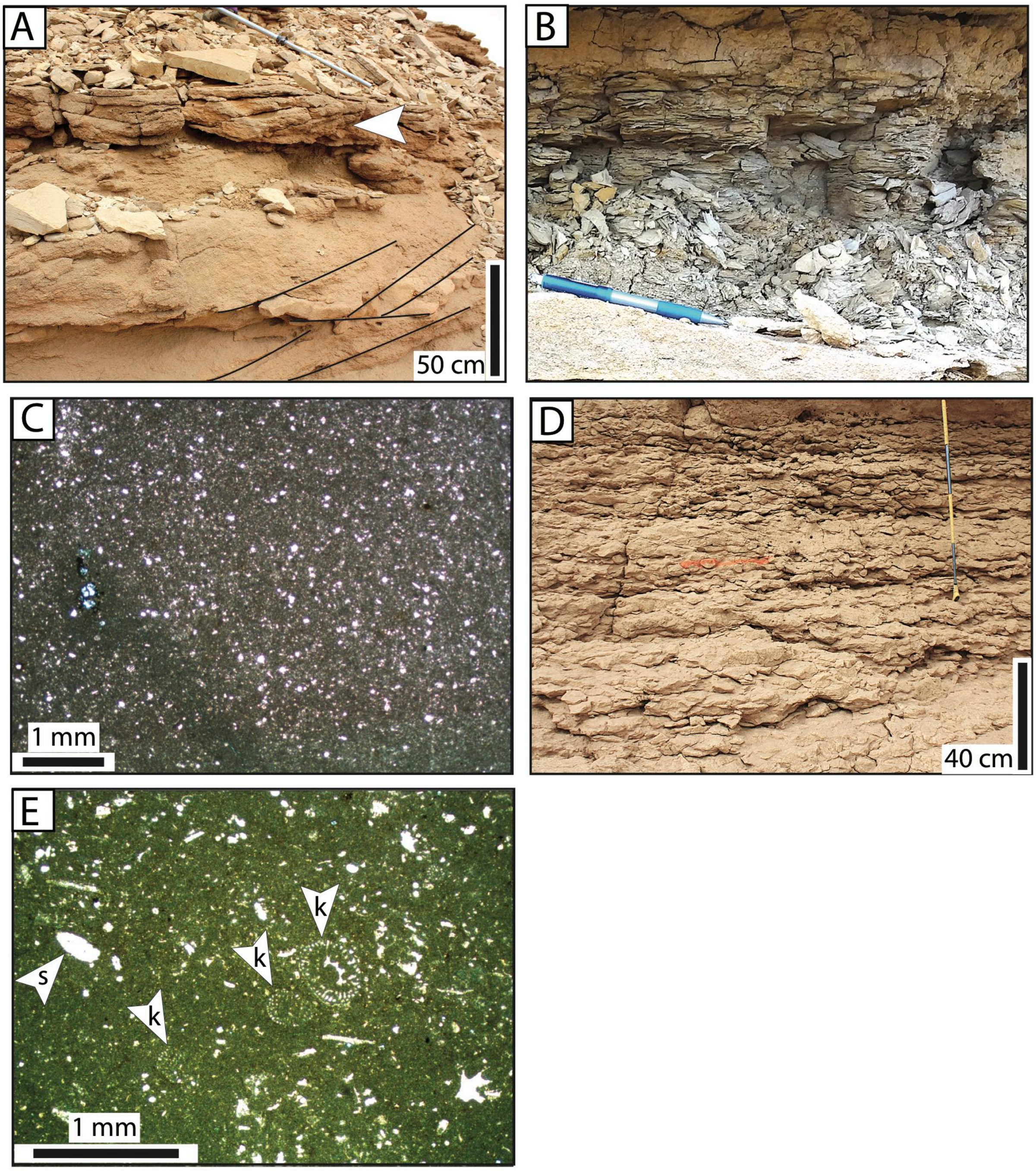

Fig. 7

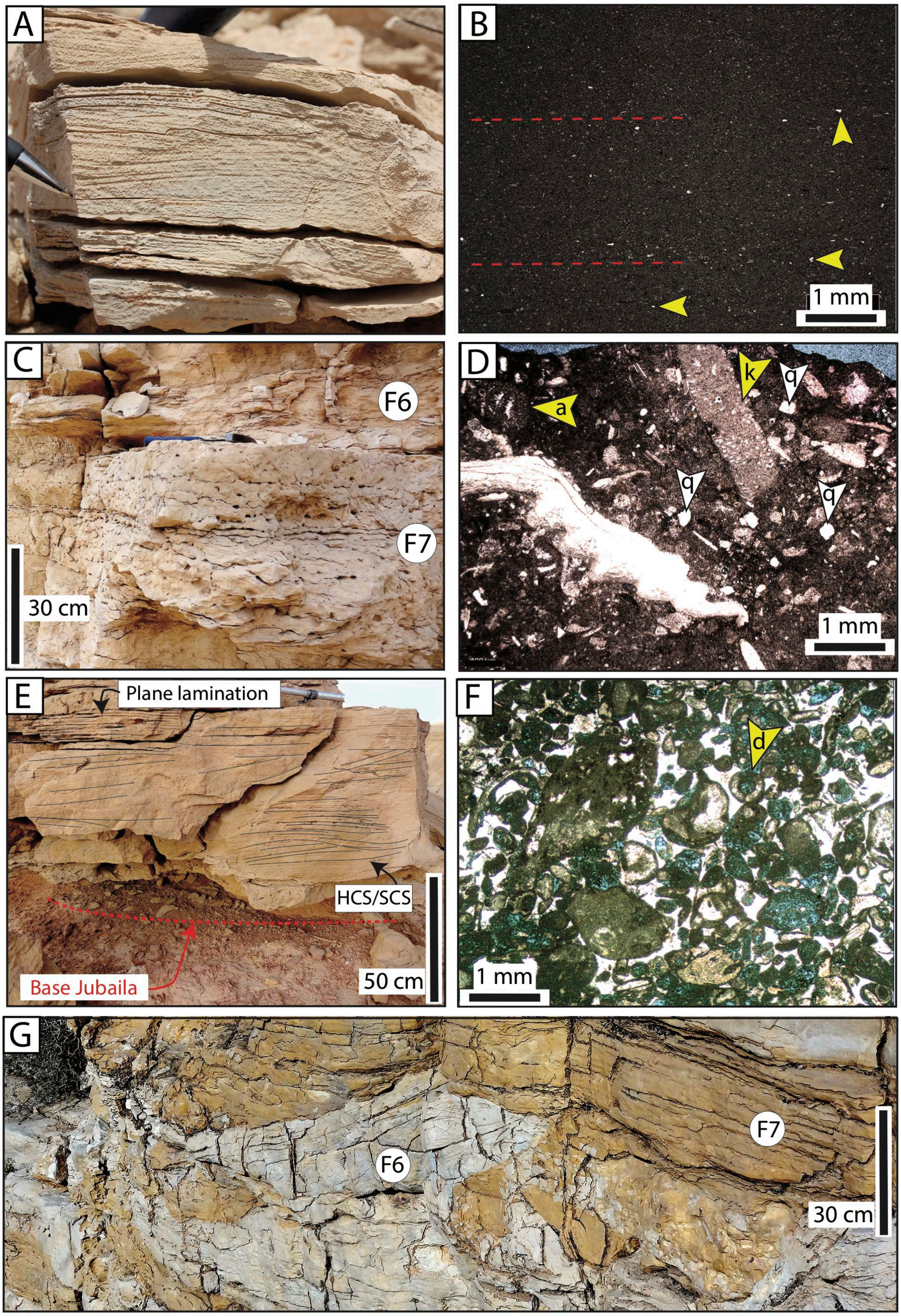
A
B
1 mm
C
F6
F7
30 cm
D
a
k
q
q
q
1 mm
E
Plane lamination
HCS/SCS
Base Jubaila
50 cm
F
d
1 mm
G
F6
F7
30 cm

Fig. 8

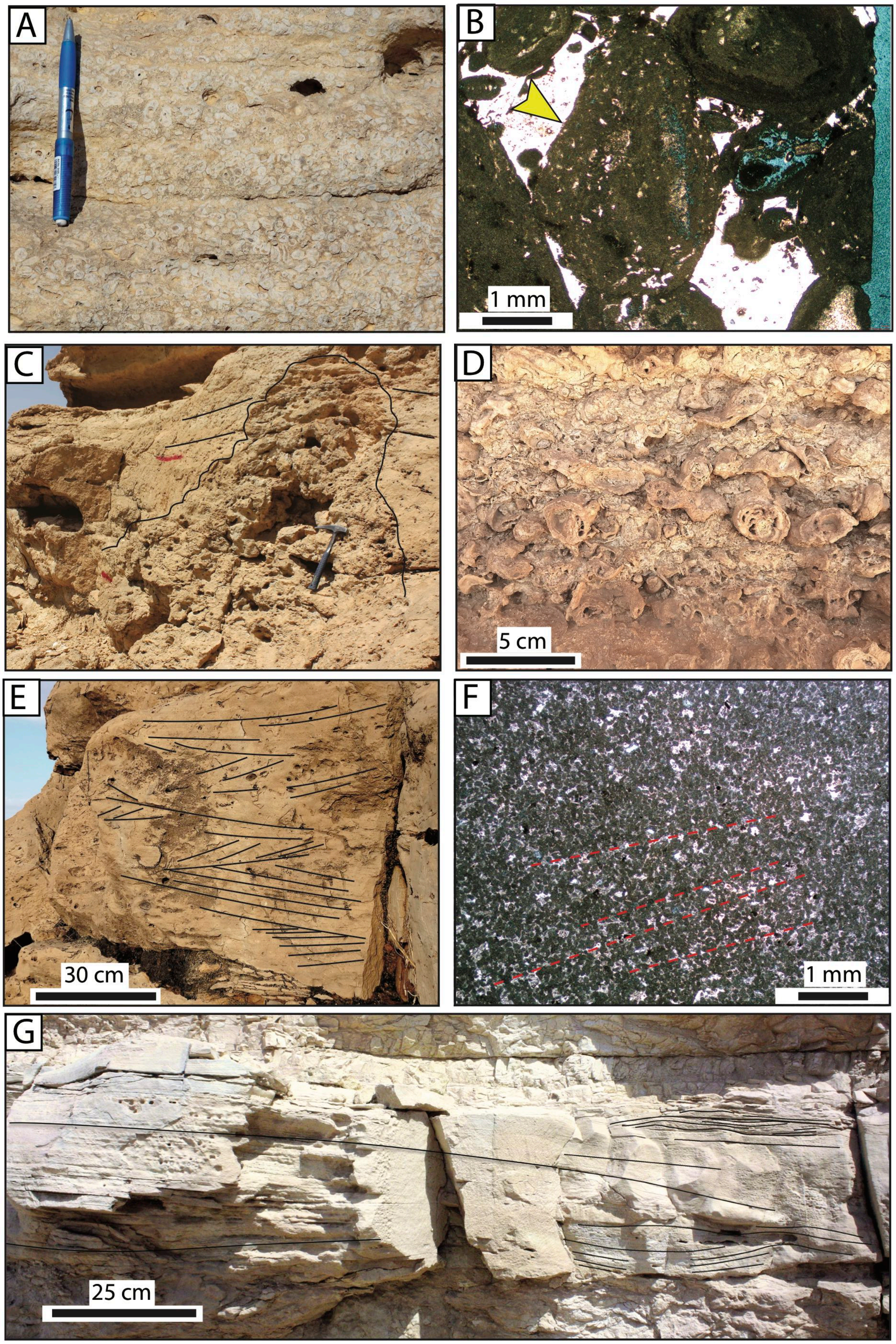

Figure. 9

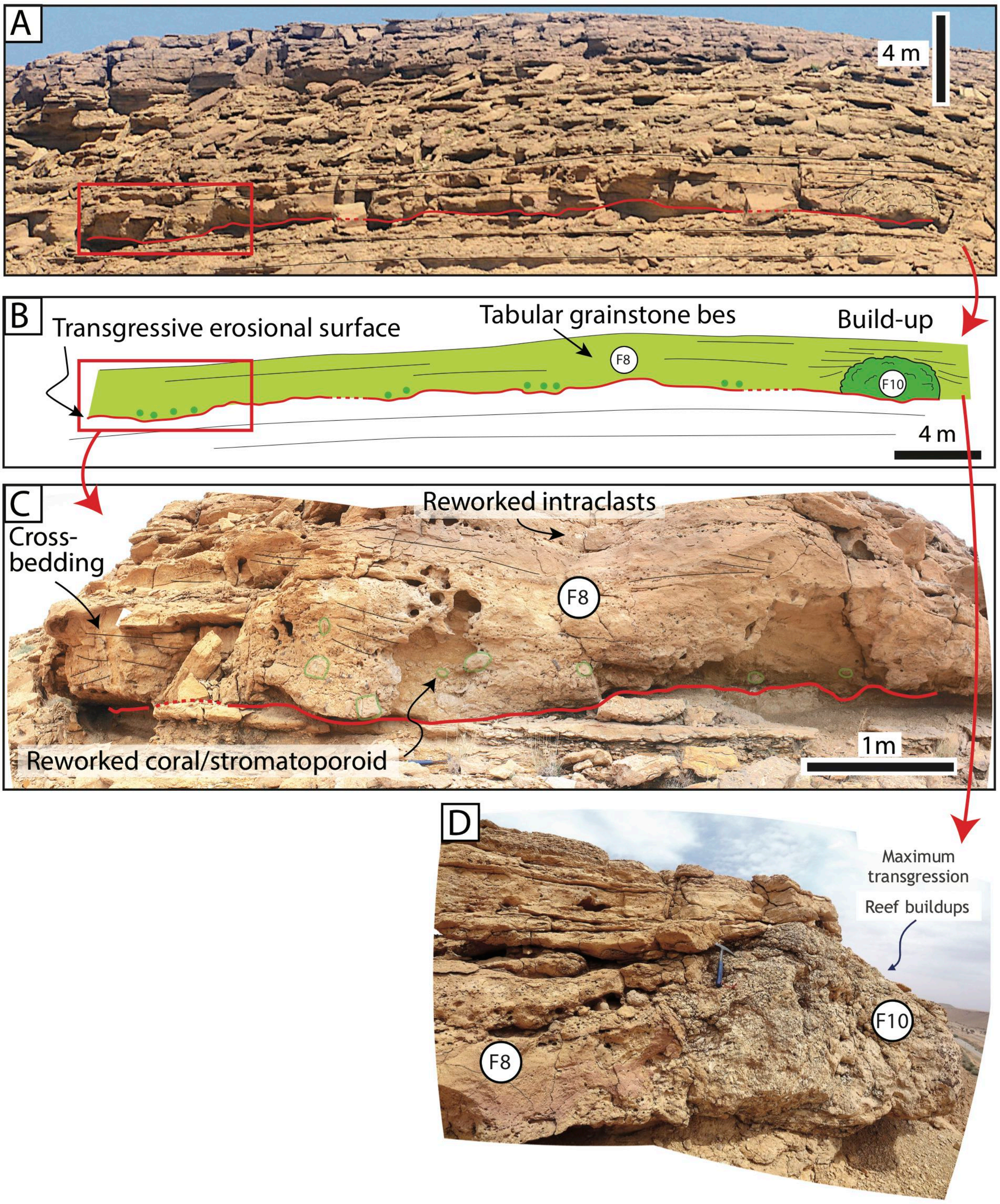

A
4 m
B
Transgressive erosional surface
Tabular grainstone bes
Build-up
F8
F10
4 m
C
Cross-
bedding
Reworked intraclasts
F8
Reworked coral/stromatoporoid
1m
D
Maximum
transgression
Reef buildups
F10
F8

Fig. 10

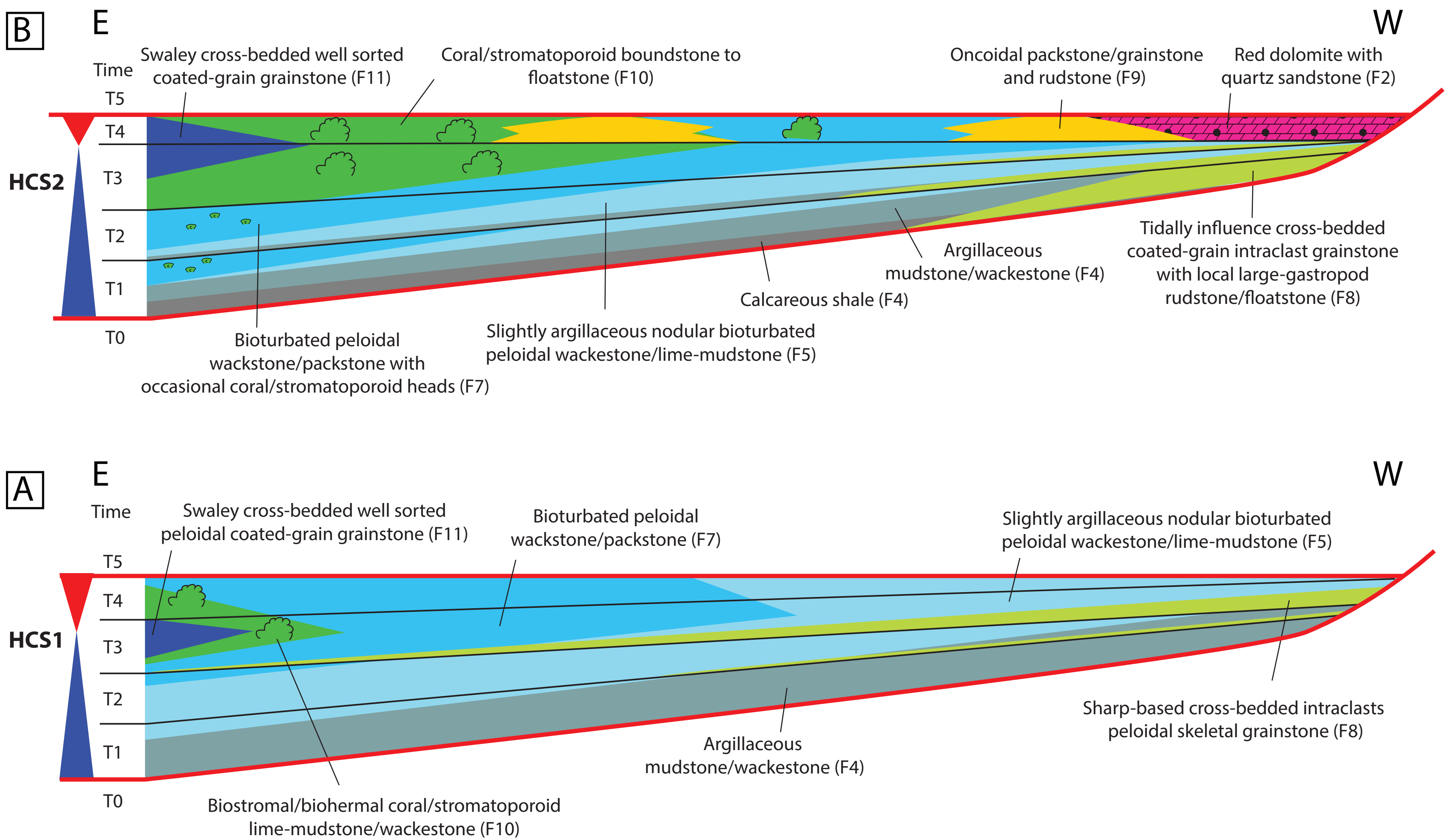

B
E
W
Time
T5
T4
T3
T2
T1
T0
HCS2
Swaley cross-bedded well sorted coated-grain grainstone (F11)
Coral/stromatoporoid boundstone to floatstone (F10)
Oncoidal packstone/grainstone and rudstone (F9)
Red dolomite with quartz sandstone (F2)
Tidally influence cross-bedded coated-grain intraclast grainstone with local large-gastropod rudstone/floatstone (F8)
Argillaceous mudstone/wackestone (F4)
Calcareous shale (F4)
Slightly argillaceous nodular bioturbated peloidal wackestone/lime-mudstone (F5)
Bioturbated peloidal wackestone/packstone with occasional coral/stromatoporoid heads (F7)
A
E
W
Time
T5
T4
T3
T2
T1
T0
HCS1
Swaley cross-bedded well sorted peloidal coated-grain grainstone (F11)
Bioturbated peloidal wackestone/packstone (F7)
Slightly argillaceous nodular bioturbated peloidal wackestone/lime-mudstone (F5)
Sharp-based cross-bedded intraclasts peloidal skeletal grainstone (F8)
Argillaceous mudstone/wackestone (F4)
Biostromal/biohermal coral/stromatoporoid lime-mudstone/wackestone (F10)

Figure 11

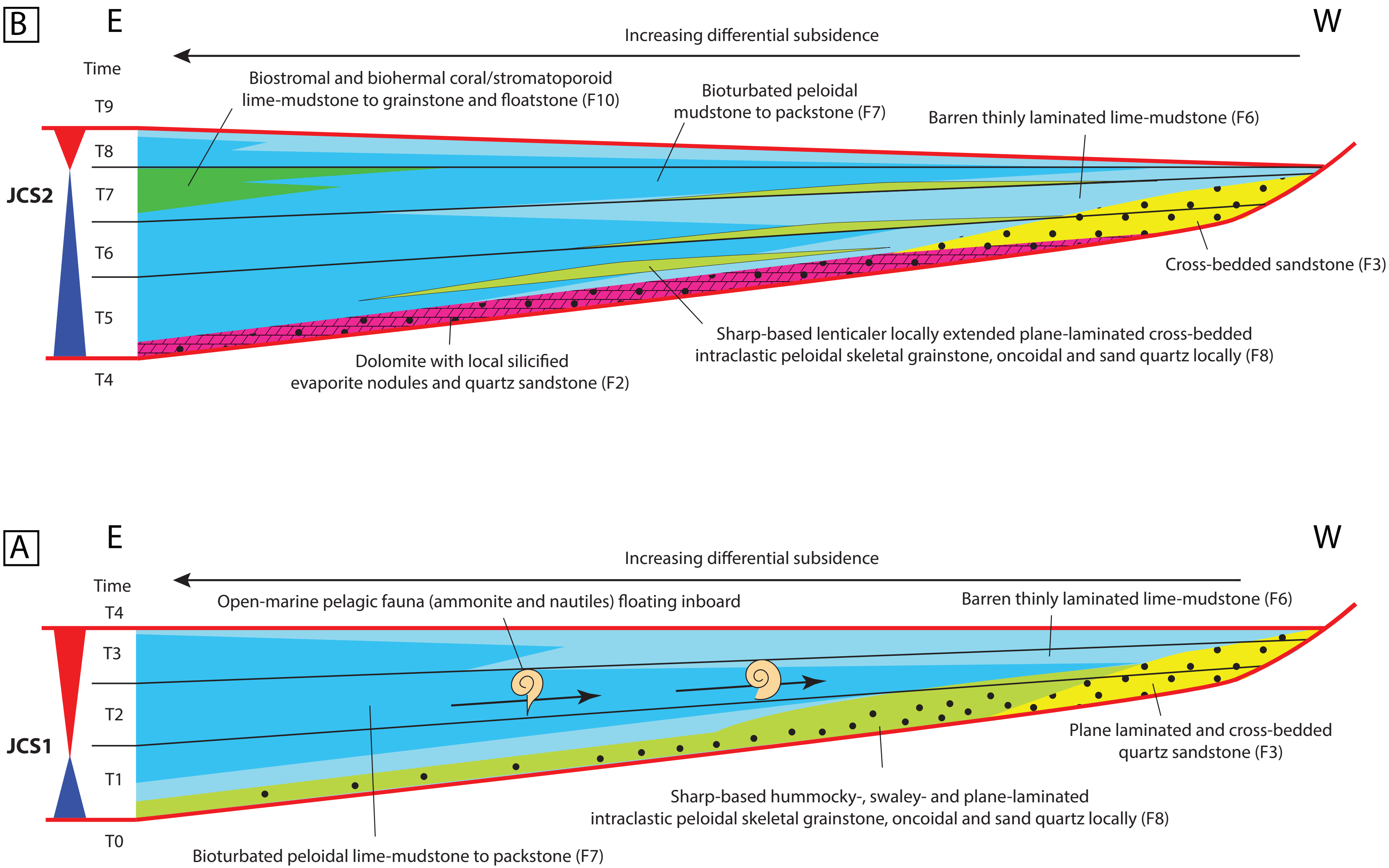
B
E
W
Increasing differential subsidence
Time
T9
T8
T7
T6
T5
T4
JCS2
Biostromal and biohermal coral/stromatoporoid
lime-mudstone to grainstone and floatstone (F10)
Bioturbated peloidal
mudstone to packstone (F7)
Barren thinly laminated lime-mudstone (F6)
Cross-bedded sandstone (F3)
Sharp-based lenticaler locally extended plane-laminated cross-bedded
intraclastic peloidal skeletal grainstone, oncoidal and sand quartz locally (F8)
Dolomite with local silicified
evaporite nodules and quartz sandstone (F2)
A
E
W
Increasing differential subsidence
Time
T4
T3
T2
T1
T0
JCS1
Open-marine pelagic fauna (ammonite and nautiles) floating inboard
Barren thinly laminated lime-mudstone (F6)
Plane laminated and cross-bedded
quartz sandstone (F3)
Sharp-based hummocky-, swaley- and plane-laminated
intraclastic peloidal skeletal grainstone, oncoidal and sand quartz locally (F8)
Bioturbated peloidal lime-mudstone to packstone (F7)

Figure 12

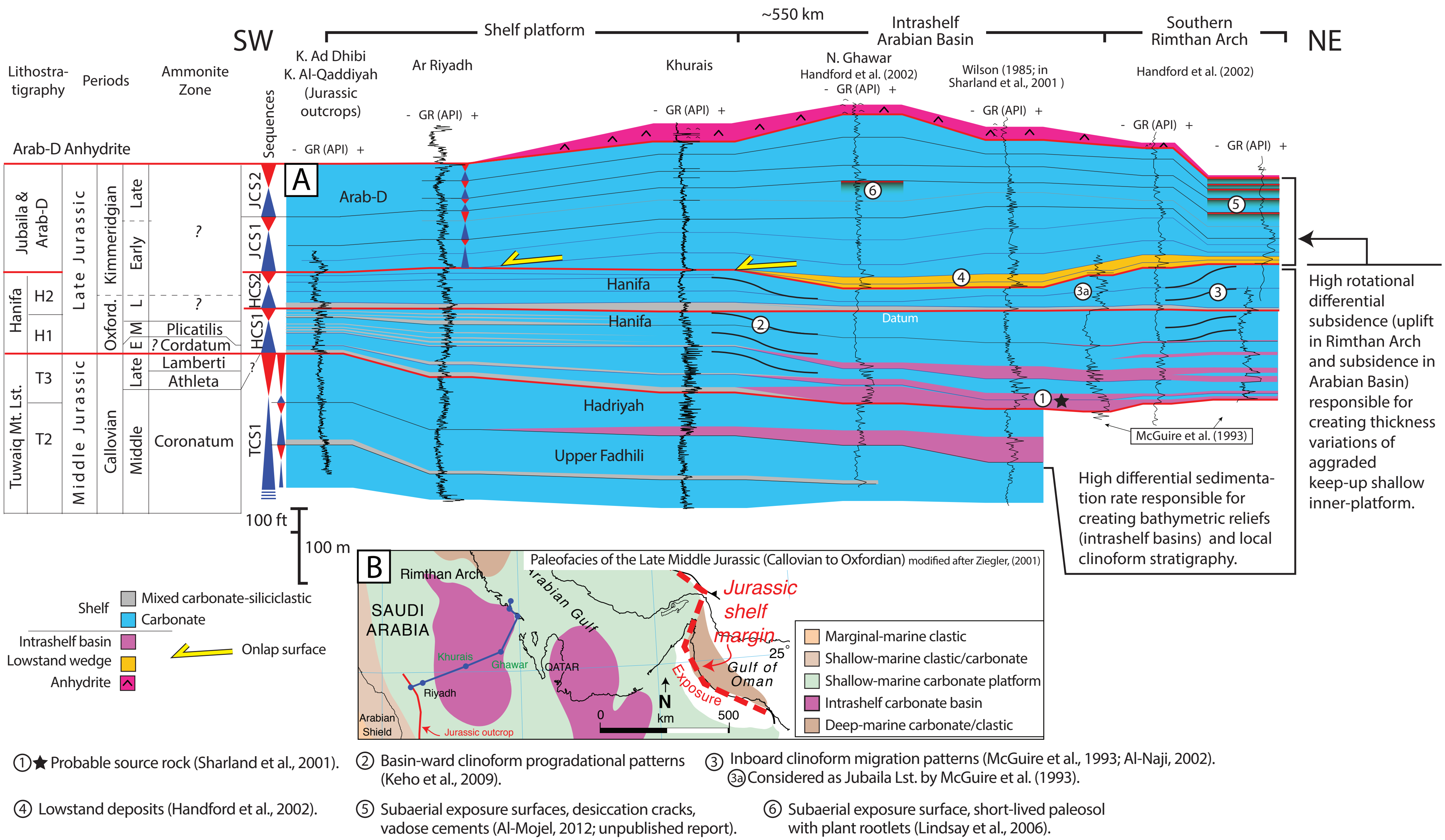
~550 km
SW
Shelf platform
Intrashelf Arabian Basin
Southern Rimthan Arch
NE
Lithostratigraphy
Periods
Ammonite Zone
Sequences
K. Ad Dhibi K. Al-Qaddiyah (Jurassic outcrops)
Ar Riyadh
Khurais
N. Ghawar Handford et al. (2002)
Wilson (1985; in Sharland et al., 2001)
Handford et al. (2002)
- GR (API) +
Arab-D Anhydrite
Jubaila & Arab-D
Hanifa
H2
H1
Tuwaiq Mt. Lst.
T3
T2
Late Jurassic
Middle Jurassic
Kimmeridgian
Oxford.
Callovian
Late
Early
L
M
E
Middle
?
Plicatilis
? Cordatum
Lamberti
Athleta
Coronatum
JCS2
JCS1
HCS2
HCS1
TCS1
A
Arab-D
Hanifa
Datum
Hadriyah
Upper Fadhili
McGuire et al. (1993)
100 ft
100 m
High differential sedimentation rate responsible for creating bathymetric reliefs (intrashelf basins) and local clinoform stratigraphy.
High rotational differential subsidence (uplift in Rimthan Arch and subsidence in Arabian Basin) responsible for creating thickness variations of aggraded keep-up shallow inner-platform.
Shelf
Mixed carbonate-siliciclastic
Carbonate
Intrashelf basin
Lowstand wedge
Anhydrite
Onlap surface
B
Paleofacies of the Late Middle Jurassic (Callovian to Oxfordian) modified after Ziegler, (2001)
Rimthan Arch
SAUDI ARABIA
Arabian Gulf
Khurais
Ghawar
QATAR
Riyadh
Arabian Shield
Jurassic outcrop
Jurassic shelf margin
Exposure
Gulf of Oman
25°
N
0
500
km
Marginal-marine clastic
Shallow-marine clastic/carbonate
Shallow-marine carbonate platform
Intrashelf carbonate basin
Deep-marine carbonate/clastic
①★ Probable source rock (Sharland et al., 2001).
② Basin-ward clinoform progradational patterns (Keho et al., 2009).
③ Inboard clinoform migration patterns (McGuire et al., 1993; Al-Naji, 2002).
③a Considered as Jubaila Lst. by McGuire et al. (1993).
④ Lowstand deposits (Handford et al., 2002).
⑤ Subaerial exposure surfaces, desiccation cracks, vadose cements (Al-Mojel, 2012; unpublished report).
⑥ Subaerial exposure surface, short-lived paleosol with plant rootlets (Lindsay et al., 2006).

Figure 13

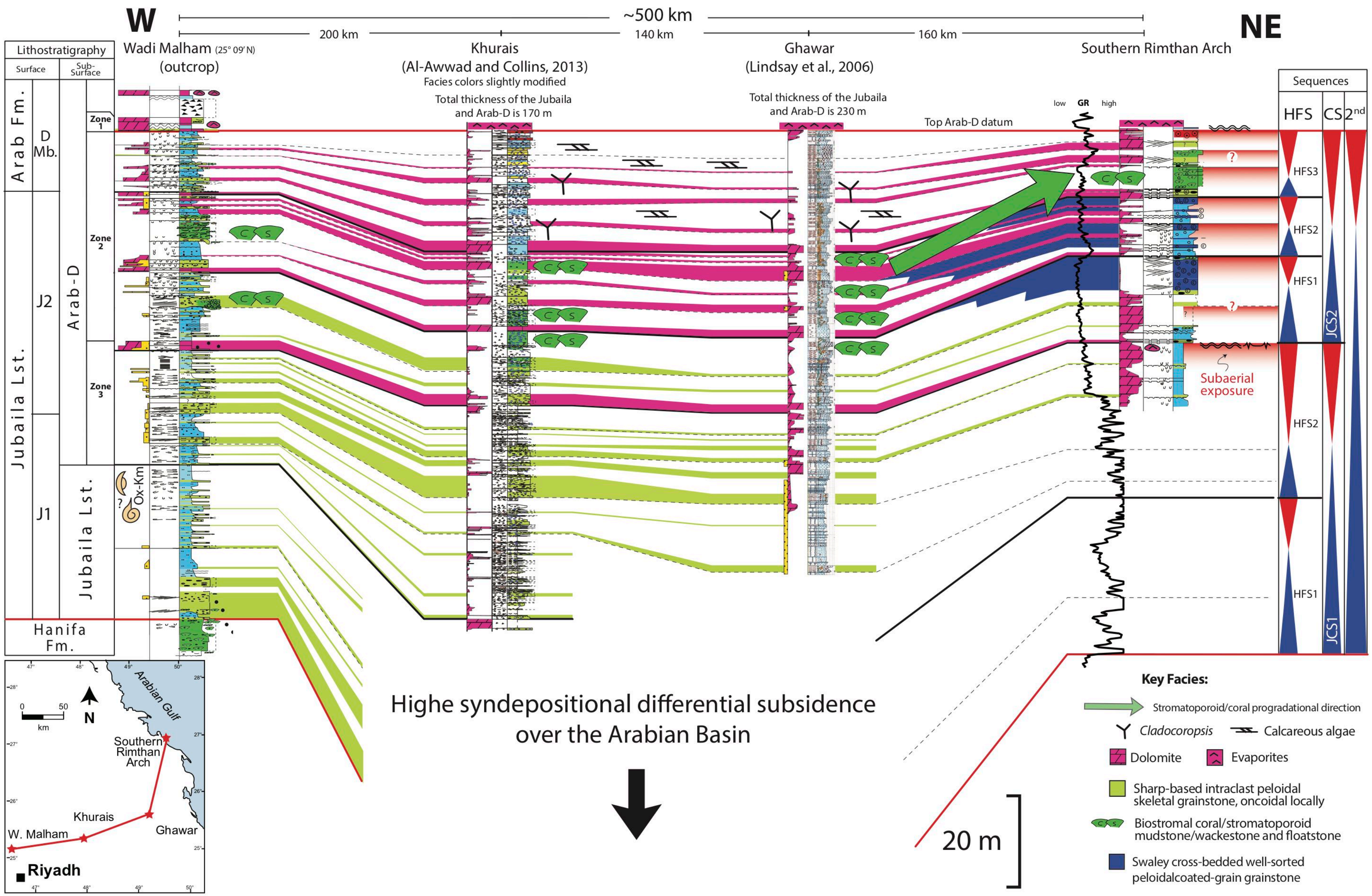
W
~500 km
NE
200 km
140 km
160 km
Lithostratigraphy
Surface
Sub-surface
Wadi Malham (25° 09' N)
(outcrop)
Khurais
(Al-Awwad and Collins, 2013)
Facies colors slightly modified
Total thickness of the Jubaila and Arab-D is 170 m
Ghawar
(Lindsay et al., 2006)
Total thickness of the Jubaila and Arab-D is 230 m
Southern Rimthan Arch
Top Arab-D datum
low GR high
Sequences
HFS
CS
2nd
Arab Fm.
D Mb.
Zone 1
Zone 2
Zone 3
Arab-D
Jubaila Lst.
J2
J1
Ox-Km
Hanifa Fm.
HFS3
HFS2
HFS1
HFS2
HFS1
JCS2
JCS1
Subaerial exposure
Highe syndepositional differential subsidence over the Arabian Basin
Key Facies:
Stromatoporoid/coral progradational direction
Cladocoropsis
Calcareous algae
Dolomite
Evaporites
Sharp-based intraclast peloidal skeletal grainstone, oncoidal locally
Biostromal coral/stromatoporoid mudstone/wackestone and floatstone
Swaley cross-bedded well-sorted peloidalcoated-grain grainstone
20 m
Arabian Gulf
N
0 50 km
Southern Rimthan Arch
Khurais
W. Malham
Ghawar
Riyadh

Figure 14

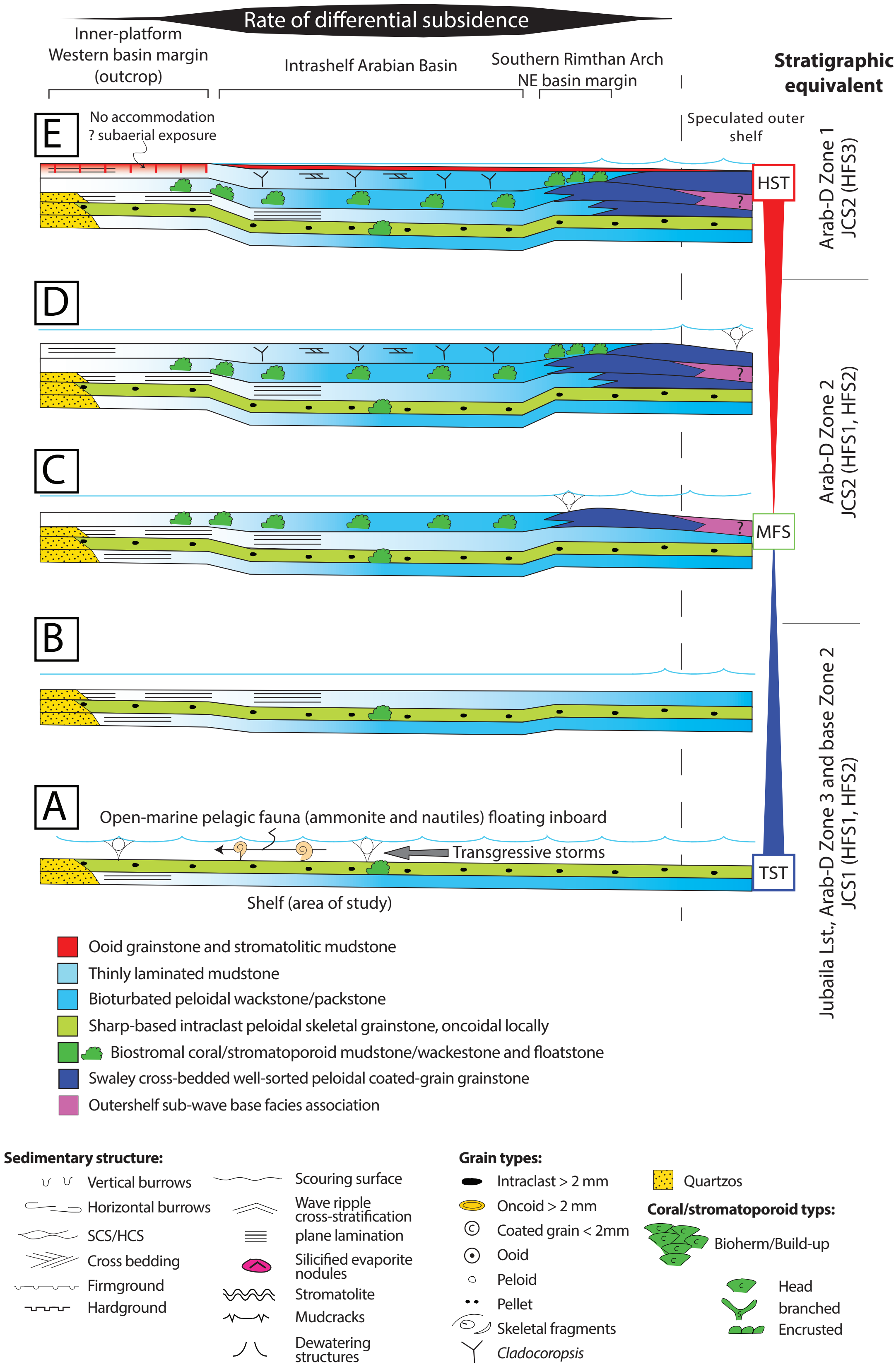

Rate of differential subsidence
Inner-platform
Western basin margin
(outcrop)
Intrashelf Arabian Basin
Southern Rimthan Arch
NE basin margin
Stratigraphic equivalent
E
No accommodation
? subaerial exposure
Speculated outer shelf
HST
Arab-D Zone 1
JCS2 (HFS3)
D
Arab-D Zone 2
JCS2 (HFS1, HFS2)
C
MFS
B
Jubaila Lst., Arab-D Zone 3 and base Zone 2
JCS1 (HFS1, HFS2)
A
Open-marine pelagic fauna (ammonite and nautiles) floating inboard
Transgressive storms
TST
Shelf (area of study)
Ooid grainstone and stromatolitic mudstone
Thinly laminated mudstone
Bioturbated peloidal wackstone/packstone
Sharp-based intraclast peloidal skeletal grainstone, oncoidal locally
Biostromal coral/stromatoporoid mudstone/wackestone and floatstone
Swaley cross-bedded well-sorted peloidal coated-grain grainstone
Outershelf sub-wave base facies association
Sedimentary structure:
Vertical burrows
Horizontal burrows
SCS/HCS
Cross bedding
Firmground
Hardground
Scouring surface
Wave ripple cross-stratification
plane lamination
Silicified evaporite nodules
Stromatolite
Mudcracks
Dewatering structures
Grain types:
Intraclast > 2 mm
Oncoid > 2 mm
Coated grain < 2mm
Ooid
Peloid
Pellet
Skeletal fragments
Cladocoropsis
Quartzos
Coral/stromatoporoid typs:
Bioherm/Build-up
Head
branched
Encrusted

Figure 15

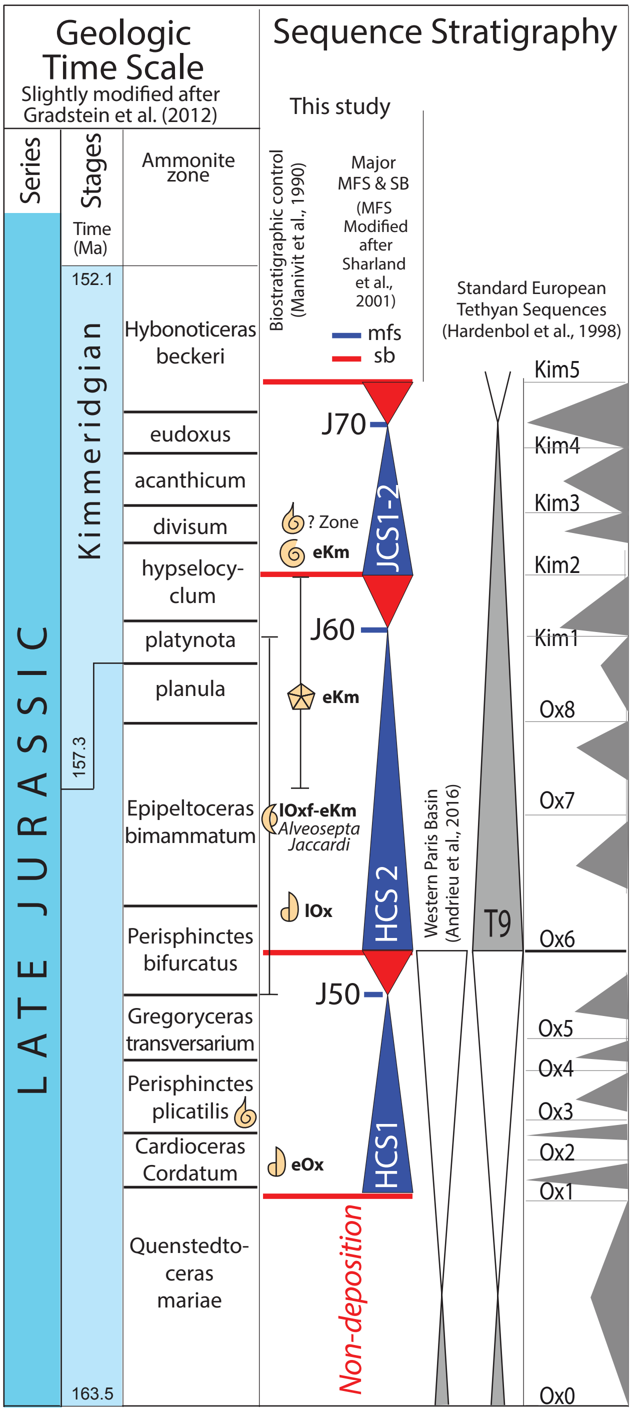
Geologic Time Scale
Slightly modified after Gradstein et al. (2012)
Sequence Stratigraphy
This study
Series
Stages
Time (Ma)
Ammonite zone
Biostratigraphic control (Manivit et al., 1990)
Major MFS & SB (MFS Modified after Sharland et al., 2001)
mfs
sb
Standard European Tethyan Sequences (Hardenbol et al., 1998)
152.1
157.3
163.5
LATE JURASSIC
Kimmeridgian
Hybonoticeras beckeri
eudoxus
acanthicum
divisum
hypselocy-clum
platynota
planula
Epipeltoceras bimammatum
Perisphinctes bifurcatus
Gregoryceras transversarium
Perisphinctes plicatilis
Cardioceras Cordatum
Quenstedto-ceras mariae
J70
J60
J50
JCS1-2
HCS 2
HCS1
? Zone
eKm
eKm
lOxf-eKm
Alveosepta Jaccardi
lOx
eOx
Non-deposition
Western Paris Basin (Andrieu et al., 2016)
T9
Kim5
Kim4
Kim3
Kim2
Kim1
Ox8
Ox7
Ox6
Ox5
Ox4
Ox3
Ox2
Ox1
Ox0

Figure 16

Table 1: Summary of sedimentary facies description.

Facies	Description
F1: Anhydrite solution collapse breccia: subaqueous salina	Cm- to dm-sized angular clasts and round molds, made up of limestone, dolomite and rare remnant of anhydrite clasts joined by very fine dolomitic matrix. Unit thickness 4 to 5 m (Fig. 6A and B).
F2: Red dolomite: tidal-flat to restricted lagoon	Mud- and grain-supported texture, fabric preserving very-fine to fine rhombic crystals, medium to coarse peloids and sandstone quartz, structureless, rare bioturbation traces, rare cross-bedding, silicified evaporite nodules, crinkly laminated structure. Unit thickness 0.3 to 2.5 m (Fig. 6C and D).
F3: Cross-bedded quartz sandstone: shallow-marine sand-flat	Medium to very coarse-grained sandstone, skeletal fragments, carbonate cement, plane-laminations, 2D mega-ripple cross-bedding, wave-ripple laminations, bioturbation. Unit thickness 0.2 to 2 m (Fig. 7A).
F4: Calcareous shale and argillaceous lime-mudstone to packstone: shale-dominated inner-lagoon	Silt-size pelletal grains, concoidal soft parting (Fig. 7B, and C), thinly laminated structure, *Chondrites* burrows, common sponge spicules (Fig. 7C), echinoderms, brachiopods and bivalves (*Pholadomya*; Manivit et al, 1990). Unit thickness 0.5 to 9 m.
F5: Nodular bioturbated peloidal wackestone/mudstone: inner lagoon	Silt-size pelletal grains and very fine to medium-grained peloids, heterolithic stratification of cm-thick of mudstone-wackestone and packstone-grainstone, wave lamination, bioturbation (*Planolites*), *Chondrites* burrows, encrusted and rare biohermal coral/stromatoporoid, echinoderms, brachiopods, benthic foraminifera (*Kurnubia Jurassica, Lenticulina* sp., *Nautiloculina oolithica*), sponge spicules. Unit thickness 1 to 11 m (Fig. 7D and E).
F6: Thinly laminated barren lime-mudstone: restricted inner-lagoon	Silt-sized pellets, very fine-grained quartz, paleontologically-barren and non-bioturbated, thin horizontal to low angle undulose lamination, rare HCS (Fig. 8A and B), wispy laminations, dewatering and soft-sediment deformations structures (Fig. 8G). Unit thickness 0.2 to 10 m thick.
F7: Bioturbated peloidal lime-mudstone to packstone	Creamy white, silt to very-fine pellets, medium-grained peloids, mudstone to packstone texture, argillaceous wispy solution seams, rare nodular structures, intense bioturbation, branched vertical burrows (*Thalassinoides*), ammonites, nautiloids, echinoderms, brachiopods, bivalves, common benthic foraminifera (*Alveosepta jacardi*; *Kurnubia jurassica, Redmondoides lugeoni*) and lesser sponge spicules, extensive tabular units up to 0.5 to 10 m thick (Fig. 8C and D).
F8: Sharp-based intraclast-peloidal skeletal grainstone, oncoidal locally: storm-dominated inner-platform	Fine to medium peloids, coarse to very-coarse coated-grains and granule to cobble sized rip-up clasts and skeletal debris, grainstones and rudstone/floatstones texture, 5 to 10% quartz silt (Hanifa Fm.), 50% quartz sand (Jubaila Lst.), plane-parallel lamination, HCS and SCS, wave ripple cross-bedding, bidirectional tidal cross-bedding, weak bioturbation, locally soft-sediment deformation, sharp bed bases with tool marks, graded-bedding, gradational bed-tops, bored encrusted hardground, current and/or wave ripple marks and trails, reworked bioclasts of echinoderms, brachiopods, gastropods (*Nerinea* sp.), dasyclads (*Clypeina*), benthic foraminifera (*Lenticulina* sp., *Kurnubia jurassica, Nautiloculina oolithica*), closely packed fitted-fabrics, extensive and tabular at outcrop scale (x100 m), slightly erosive, gentle channelized geometries, decimeter-thick individual beds, meter-thick staked sets (Fig. 8E and F).
F9: Oncoidal packstone, grainstone and rudstone: oncoidal bars/shoal	Coarse to very-coarse coated-grains and skeletal fragments, granule- to pebble-sized oncoids (type 2 and type 3; *sensu* Védrine et al., 2007), decimeter-scale cross-bedding and vertical burrows, but can also be structureless, reworked coral/stromatoporoid heads and some calci-sponges (*Cladocoropsis*), dasyclads (*Clypeina*), benthic foraminifera (Miliolid, *Kurnubia jurassica, Redmondoides lugeoni*). Lenticular but locally extended units up to 0.25 to 2 m thick (Fig. 9A and B).
F10: Coral/stromatoporoid boundstone to floatstone: low-energy and high-energy back-barrier	Medium peloids, coarse skeletal fragments, cobble-sized coral/stromatoporoid and rudists (Fig. 9D), boundstone, grainstone and floatstone texture, massive and sometimes highly bioturbated, occasional microbial laminated fabric, *Cladocoropsis* and benthic foraminifera (*Alveosepta jacardi, Kurnubia jurassica, Redmondoides lugeoni*). Patch-reefs up to 15 m in diameter and 4 m in thickness (in Hanifa Fm.; Fig. 9C) and up to 4 m in diameter and 2 m in thickness in the upper Jubaila Limestone (Fig. 10). Unit thickness 1.5 to 8 m thick.
F11: Cross-bedded coated-grain and peloidal grainstone: shoal and washover complex	Very-fine to fine peloids, medium coated-grain grainstones, fragments of echinoderms, brachiopods and gastropods, trough cross-bedding, hummocky cross-stratification (HCS) and swaley cross stratification (SCS), plane lamination, occasional intense bioturbation, tabular and channelized units up to 0.4 to 7 m thick (Fig. 9E, F and G).

Appendix 1

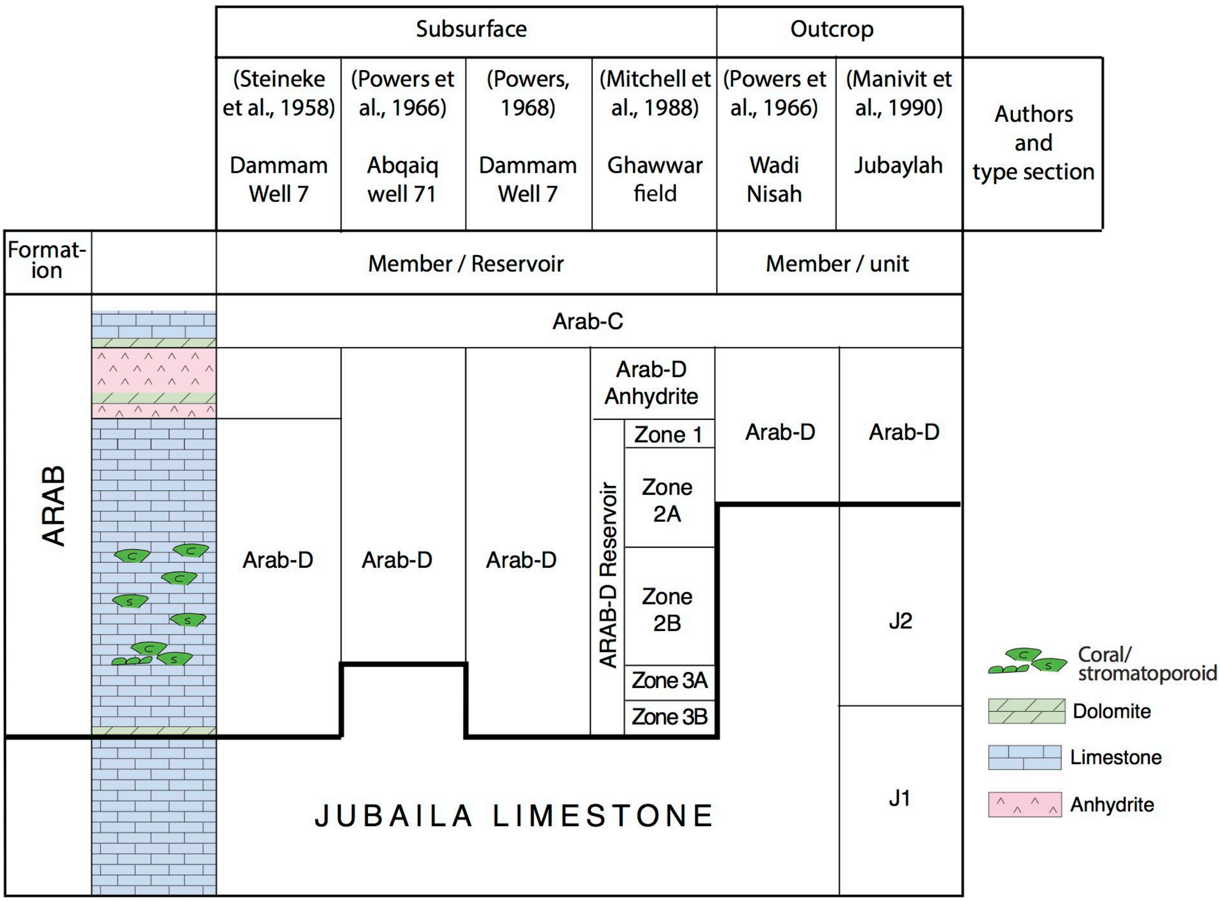

Appendix 1: Table shows the definitions of the Jubaila-Arab-D lithostratigraphic contact among different authors. This study follows Manivit et al. (1990). (Modified from Meyer et al 1996).

Appendix 2:
Khashm Al Qaddiyah section, Hanifa Formation
Riyadh-Mecca highway road-cut

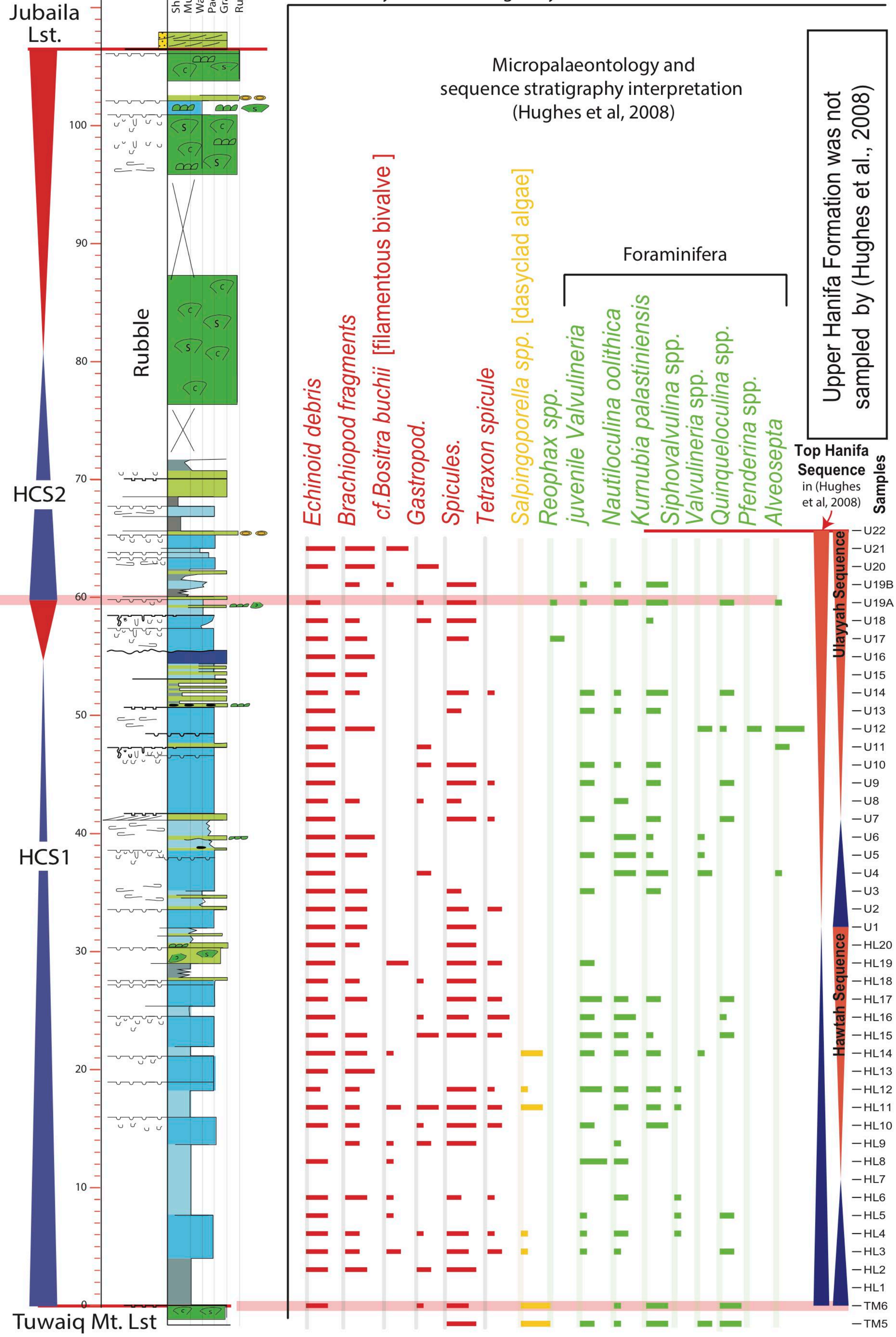

Appendix 3:
Sedimentological log and semi-quantitative micropalaeontological analysis of the Hanifa Formation, Wadi Birk

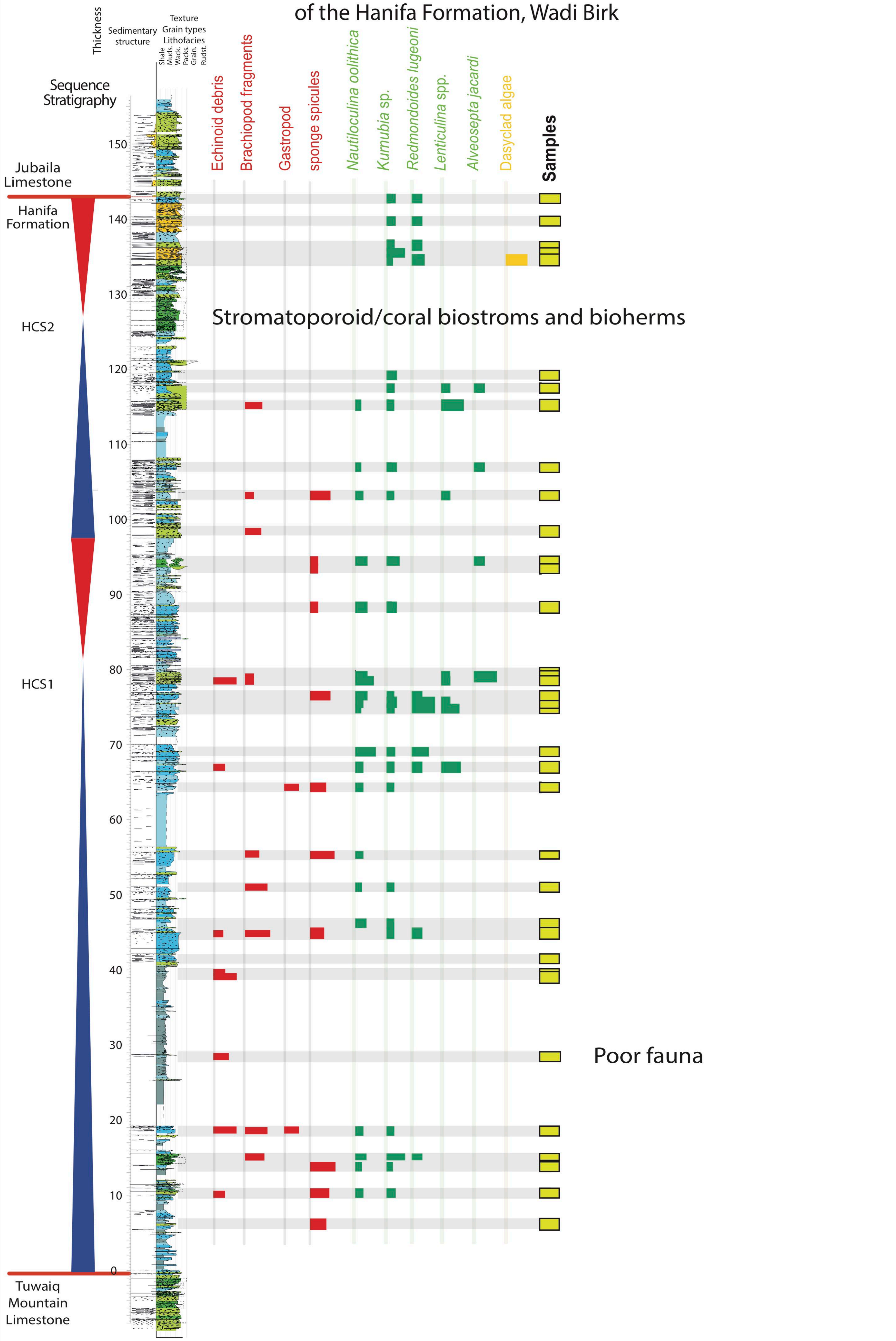

Appendix 4:
Sedimentological log and semi-quantitative micropalaeontological analysis of the Jubaila Limestone, Wadi Birk

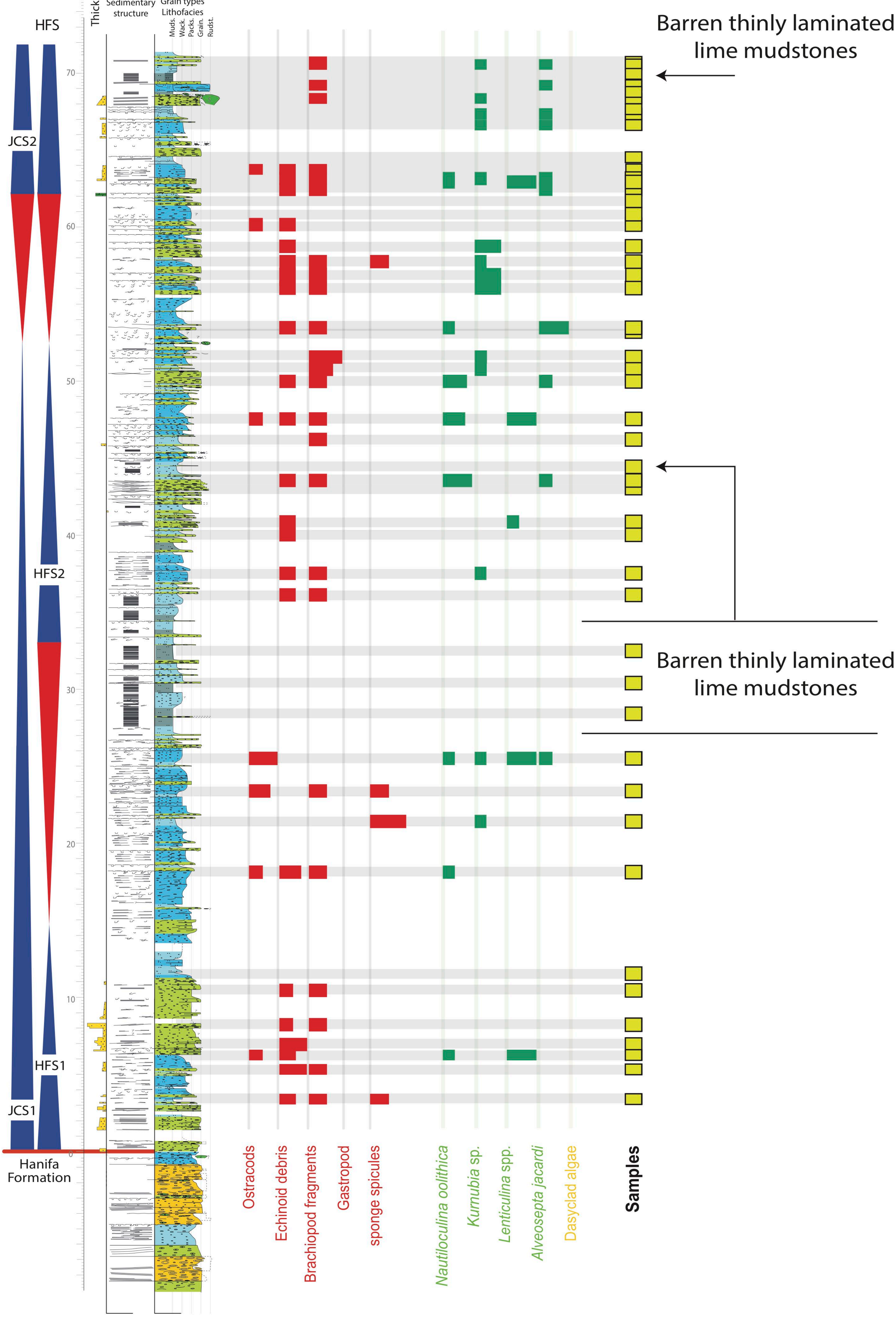

Table 1 Summary of sedimentary facies description.

Facies	Description
F1: Anhydrite solution collapse breccia: subaqueous salina	Cm- to dm-sized angular clasts and round molds, made up of limestone, dolomite and rare remnant of anhydrite clasts joined by very fine dolomitic matrix. Unit thickness 4 to 5 m (Fig. 6A and B).
F2: Red dolomite: tidal-flat to restricted lagoon	Mud- and grain-supported texture, fabric preserving very-fine to fine rhombic crystals, medium to coarse peloids and sandstone quartz, structureless, rare bioturbation traces, rare cross-bedding, silicified evaporite nodules, crinkly laminated structure. Unit thickness 0.3 to 2.5 m (Fig. 6C and D).
F3: Cross-bedded quartz sandstone: shallow-marine sand-flat	Medium to very coarse-grained sandstone, skeletal fragments, carbonate cement, plane-laminations, 2D mega-ripple cross-bedding, wave-ripple laminations, bioturbation. Unit thickness 0.2 to 2 m (Fig. 7A).
F4: Calcareous shale and argillaceous lime-mudstone to packstone: shale-dominated inner-lagoon	Silt-size pelletal grains, concoidal soft parting (Fig. 7B, and C), thinly laminated structure, *Chondrites* burrows, common sponge spicules (Fig. 7C), echinoderms, brachiopods and bivalves (*Pholadomya*; Manivit et al, 1990). Unit thickness 0.5 to 9 m.
F5: Nodular bioturbated peloidal wackestone/mudstone: inner lagoon	Silt-size pelletal grains and very fine to medium-grained peloids, heterolithic stratification of cm-thick of mudstone-wackestone and packstone-grainstone, wave lamination, bioturbation (*Planolites*), *Chondrites* burrows, encrusted and rare biohermal coral/stromatoporoid, echinoderms, brachiopods, benthic foraminifera (*Kurnubia Jurassica, Lenticulina* sp., *Nautiloculina oolithica*), sponge spicules. Unit thickness 1 to 11 m (Fig. 7D and E).
F6: Thinly laminated barren lime-mudstone: restricted inner-lagoon	Silt-sized pellets, very fine-grained quartz, paleontologically-barren and non-bioturbated, thin horizontal to low angle undulose lamination, rare HCS (Fig. 8A and B), wispy laminations, dewatering and soft-sediment deformations structures (Fig. 8G). Unit thickness 0.2 to 10 m thick.
F7: Bioturbated peloidal lime-mudstone to packstone	Creamy white, silt to very-fine pellets, medium-grained peloids, mudstone to packstone texture, argillaceous wispy solution seams, rare nodular structures, intense bioturbation, branched vertical burrows (*Thalassinoides*), ammonites, nautiloids, echinoderms, brachiopods, bivalves, common benthic foraminifera (*Alveosepta jacardi*; *Kurnubia jurassica, Redmondoides lugeoni*) and lesser sponge spicules, extensive tabular units up to 0.5 to 10 m thick (Fig. 8C and D).

F8: Sharp-based intraclasts peloidal skeletal grainstone, oncoidal locally: storm-dominated inner-platform	Fine to medium peloids, coarse to very-coarse coated-grains and granule to cobble sized rip-up clasts and skeletal debris, grainstones and rudstone/floatstone texture, 5 to 10% quartz silt (Hanifa Fm.), 50% quartz sand (Jubaila Lst.), plane-parallel lamination, HCS and SCS, wave ripple cross-bedding, bidirectional tidal cross-bedding, weak bioturbation, locally soft-sediment deformation, sharp bed bases with tool marks, graded-bedding, gradational bed-tops, bored encrusted hardground, current and/or wave ripple marks and trails, reworked bioclasts of echinoderms, brachiopods, gastropods (*Nerinea* sp.), dasyclads (*Clypeina*), benthic foraminifera (*Lenticulina* sp., *Kurnubia jurassica, Nautiloculina oolithica*), closely packed fitted-fabrics, extensive and tabular at outcrop scale (x100 m), slightly erosive, gentle channelized geometries, decimeter-thick individual beds, meter-thick staked sets (Fig. 8E and F).
F9: Oncoidal packstone, grainstone and rudstone: oncoidal bars/shoal	Coarse to very-coarse coated-grains and skeletal fragments, granule- to pebble-sized oncoids (type 2 and type 3; *sensu* Védrine et al., 2007), decimeter-scale cross-bedding and vertical burrows, but can also be structureless, reworked coral/stromatoporoid heads and some calci-sponges (*Cladocoropsis*), dasyclads (*Clypeina*), benthic foraminifera (Miliolid, *Kurnubia jurassica, Redmondoides lugeoni*). Lenticular but locally extended units up to 0.25 to 2 m thick (Fig. 9A and B).
F10: Coral/stromatoporoid boundstone to floatstone: low-energy and high-energy back-barrier	Medium peloids, coarse skeletal fragments, cobble-sized coral/stromatoporoid and rudists (Fig. 9D), boundstone, grainstone and floatstone texture, massive and sometimes highly bioturbated, occasional microbial laminated fabric, *Cladocoropsis* and benthic foraminifera (*Alveosepta jacardi, Kurnubia jurassica, Redmondoides lugeoni*). Patch-reefs up to 15 m in diameter and 4 m in thickness (in Hanifa Fm.; Fig. 9C) and up to 4 m in diameter and 2 m in thickness in the upper Jubaila Limestone (Fig. 10). Unit thickness 1.5 to 8 m thick.
F11: Cross-bedded coated-grain and peloidal grainstone: shoal and washover complex	Very-fine to fine peloids, medium coated-grain grainstones, fragments of echinoderms, brachiopods and gastropods, trough cross-bedding, hummocky cross-stratification (HCS) and swaley cross stratification (SCS), plane lamination, occasional intense bioturbation, tabular and channelized units up to 0.4 to 7 m thick (Fig. 9E, F and G).